OCEAN CIRCULATION AND TEMPERATURE PREDICTION MODEL: I. THE PACIFIC

R. C. Alexander

RAND Corporation

Prepared for:

Defense Advanced Research Projects Agency

October 1973

ARPA ORDER NO.: 189-1
3P10 Distributed Information Systems

R-1296-ARPA
October 1973

Ocean Circulation and Temperature Prediction Model: I. The Pacific

R. C. Alexander

A Report prepared for

DEFENSE ADVANCED RESEARCH PROJECTS AGENCY

25th Year
Rand
SANTA MONICA, CA. 90406

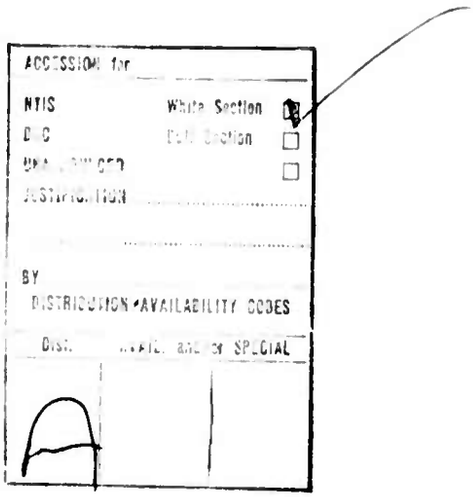

The research described in this Report was sponsored by the Defense Advanced Research Projects Agency under contract No. DAHC15-73-C-0181. Reports of The Rand Corporation do not necessarily reflect the opinions or policies of the sponsors of Rand research.

ARPA ORDER NO.: 189-1
3P10 Distributed Information Systems

R-1296-ARPA
October 1973

Ocean Circulation and Temperature Prediction Model: I. The Pacific

R. C. Alexander

A Report prepared for

DEFENSE ADVANCED RESEARCH PROJECTS AGENCY

Rand
SANTA MONICA, CA. 90406

PREFACE

This is one of a series of reports on research and development being carried out under the Rand/ARPA Climate Dynamics Project. While other reports have given research or experimental results, the present report is aimed primarily at development, specifically model improvement in one important area: the need for an interactive world ocean model for climate experiments in conjunction with the Mintz-Arakawa atmospheric general circulation model. This report concentrates on formulation of the basic ocean model, with application to the Pacific. Generalization to the world ocean and coupling with the atmospheric counterpart will be treated in separate publications.

At least two previous Rand publications provided direct inputs to the present work:

RM-6211-ARPA, *Numerical Studies of Planetary Circulations in a Wind-Driven Ocean on the Sphere.*

R-505-ARPA, *A Calibrated Analytical Model for the Thermohaline and Wind-Driven Circulation in the Interior of a Subtropical Ocean.*

Other Rand publications on ocean circulations include:

RM-5594-NSF, *The Ekman Vertical Velocity in an Enclosed β-Plane Ocean.*

RM-6110-RC, *The Effects of Western Coastal Orientation on Rossby-Wave Reflection and the Resulting Large Scale Oceanic Circulation.*

RM-6210-ARPA, *A Note on the Lateral Eddy Viscosity Due to Transient Rossby Waves in a Barotropic Model.*

The Climate Dynamics Project is sponsored by the Defense Advanced Research Projects Agency.

SUMMARY

PURPOSE

This research was undertaken to develop a numerical model for monthly and seasonal predictions of temperatures and velocities in the upper layers of the ocean. The Pacific model represents one phase in the development of a world ocean model for climate dynamics experiments with a coupled atmospheric model.

NUMERICAL MODEL

The circulation and temperature distribution in the upper layers of the Pacific Ocean are simulated by a two-level numerical model with a horizontal bottom at 300 m depth. The model is based on the primitive Eulerian equations and contains a free upper surface. The motion is driven by prescribed distributions of surface heating and wind stress, and is retarded by frictional stresses at the bottom and at the coasts. An explicit numerical scheme is used which employs central space- and time-differences with the exception that the diffusion terms are lagged one time step for stability.

Solutions for temperature and velocity are sought as an initial value problem. Initial conditions are nondivergent and geostrophic for prescribed initial temperature fields. Initialization is completed by barotropic spinup of the model while holding the initial temperature and wind stress fixed. Predictions can then be made by introducing the temperature prediction equation together with surface heating, and by allowing temporal variations of wind stress.

DEMONSTRATION RUN

The demonstration run reported here employs January climatological distributions of temperature, wind stress, and heating as initial and boundary data. Initialization gives strong flow in the equatorial region having a velocity reversal with depth, in rough agreement with observation. However, the north-south components are too large because of an inaccurate specification of initial temperature in low latitudes,

where data are sparse. A 15-day prediction with the model shows the simultaneous development of more realistic temperatures and velocities in the equatorial zone, including a relatively cold geographic equator with colder water toward the east, and very nearly zonal flow directed westward at the upper level, eastward at the lower level. However, countercurrents displaced north or south of the equator are not discerned in the results, and some features of the flow near eastern boundaries may be unrealistic.

Although the demonstration run reported here represents only a special case, the results found in the equatorial zone are typical of results found from many experiments made with this and simpler versions of the model.

CONCLUSIONS

- A main conclusion from the point of view of climate dynamics is that an oceanic general circulation model *can* make 15-day predictions showing appreciable changes in temperature distributions, at least in low latitudes. This may have important implications for monthly and seasonal simulations with interacting atmospheric and oceanic models.
- Deficiencies in the results can for the most part be traced to known limitations of the model design. These include problems of resolution near boundaries and across the equator, and the lack of continental shelf topography. The limitations are probably not serious in light of the limitations of existing atmospheric general circulation models.
- The results are generally encouraging, largely because of the realism of the predicted large-scale temperature anomaly in the eastern tropics. Moreover, computer times are modest compared with those required for a two-level atmospheric model. The Pacific model is being extended to the world ocean case, with possible improvements postponed to later.
- From an oceanographic viewpoint, the results indicate that the occurrence of zonal flow near the equator is intimately

related to the thermal structure. In particular, an east-west temperature gradient is required by the model. However, a physical explanation is not offered here, and further study with a more specialized model is required to clarify this point.

ACKNOWLEDGMENTS

I am indebted to many Rand colleagues, notably Larry Gates for his encouragement and valuable comments. Larry's homogeneous ocean model and careful researches with that model formed a basis for the present baroclinic model. My appreciation and admiration to Al Nelson for his programming of both the model and the graphics display programs. My admiration also to David Pass for finding a way to speed up the model calculations. To Phyllis Davidson, Florence Duley, and Mary Wissel my sincere thanks for typing and retyping both the present text and various earlier notes that later became part of this report. I also wish to thank Prof. Terry Williams of the Naval Postgraduate School for valuable discussions and comments during the course of the investigation. Finally, I am grateful, again, to Larry Gates and to Kent Gilbert for critically reviewing the typescript.

CONTENTS

SYMBOLS

$\underset{\sim}{(\ )}$ = a vector quantity ( ) is underscored with a tilde

A_h = constant horizontal eddy thermal conductivity

A_m = constant horizontal eddy kinematic viscosity

H = constant total mean depth

K = bottom friction coefficient

Q_s = total vertical heat flux at the air-sea interface, positive downward

Q_k^* = total vertical heat transport at level k

T = temperature

T_k = temperature at level k

$\underset{\sim}{U}_k$ = horizontal velocity vector, vertically averaged for layer k

U_k, V_k = eastward, northward components of $\underset{\sim}{U}_k$

a = earth's mean radius

c_p = specific heat of sea water at constant pressure

f = coriolis parameter, $2\Omega \sin\varphi + (u \tan\varphi)/a$

g = gravitational acceleration

h_k = constant mean thickness of layer k

i,j,k = discrete indices denoting eastward, northward, and downward position

$\underset{\sim}{k}$ = unit vertical vector, positive upward

$\underset{\sim}{n}$ = unit normal vector, positive outward

p = pressure

p_a = atmospheric pressure

q = penetrating solar radiation source term in heat flux

t = time

u,v,w = eastward, northward, and upward velocity components

$\underset{\sim}{v}$ = horizontal velocity vector

w_k = vertical velocity at level k, positive upwards

w_s = vertical velocity at the air-sea interface

z = vertical coordinate, positive upward with respect to mean sea level

α = coefficient of thermal expansion

Δt = time increment

$\Delta\lambda, \Delta\varphi$ = east-west and north-south grid spacing

ζ = elevation of air-sea interface with respect to mean sea level

θ_k = vertically averaged temperature for layer k

κ = constant vertical eddy thermal conductivity

λ = longitude

λ_i = discrete longitudinal location of grid points

ν = constant vertical eddy kinematic viscosity

π_k = vertically averaged pressure for layer k

ρ = density at constant pressure and salinity

ρ_∞ = reference density

$\underset{\sim}{\tau}_b$ = bottom stress vector

$\underset{\sim}{\tau}_s$ = wind stress vector

$\underset{\sim}{\tau}_k^*$ = total vertical transport of horizontal momentum at level k

$\tau^\lambda, \tau^\varphi$ = eastward, northward components of stress vectors

φ = latitude

φ_j = discrete latitudinal location of grid points

Ω = earth's rotation rate

I. INTRODUCTION

The world ocean forms a vast and important connecting link to the atmospheric heat engine, and hence to climatic changes, via exchanges of heat, momentum, and water vapor across the air-sea interface. Among the many interactions on many scales of motion and time, that of "wind-stress driving/sea-temperature changing" appears crucial for more accurate prediction of large-scale circulations resulting from, say, some environmental perturbation. Changes in atmospheric wind stresses acting on the ocean cause changes in transports of heat in the latter, which changes the sea temperature. This changes the distributions of heat and water vapor fluxes between ocean and atmosphere which, in turn, changes atmospheric wind patterns. Although this is understood in a rough, qualitative way, more precise information is needed in studies of climatic changes. The cause of the changed wind stress pattern may have its origin in some remote region of the globe; we need to know how much the sea temperature changes, and where and how soon, and we need to know more precisely the effect, in turn, on the atmosphere.

One approach to studying such large-scale climatic effects and interactions is by numerical modeling of the combined atmosphere-ocean system. Numerical models of the global atmosphere are already well established and operational. The better known models in this country include those of the Geophysical Fluid Dynamics Laboratory (Smagorinsky et al. 1965), the National Center for Atmospheric Research (Kasahara and Washington 1971), and the University of California at Los Angeles (Mintz 1968, Gates et al. 1971). Sea temperatures in these models have been specified climatologically, however, and there has been no fully interacting ocean.

The development of comparable ocean models began somewhat later, notably with the work of Bryan and Cox (1967, 1968), and has not yet matured. The process of coupling an oceanic model to its atmospheric counterpart presents further problems. Pioneering efforts in this direction have been made by Manabe and Bryan (Manabe 1969), who studied a simple interacting model of atmospheric flow over a single rectangular

ocean and a comparably idealized land distribution. More recently, Bryan and Cox (1972) have presented results from their noninteracting world ocean model for the case of a homogeneous ocean.

In their pioneering ocean modeling, Bryan and Cox placed more emphasis on studying the ocean in its own right (and properly so) over long periods of ocean time, and perhaps less on developing a somewhat cruder ocean model for routine use in studying the joint atmosphere-ocean system. Changes occur very slowly in the deep ocean, with time periods measurable in centuries. To make such time-integrations feasible on existing computing machines, Bryan and Cox adopted a rigid lid approximation in which the vertical velocity is set identically zero at the (level) sea surface. This effectively removes surface gravity waves, apparently without appreciably affecting the resulting *steady* circulation patterns, and thereby allows time increments to be orders of magnitude larger than would otherwise have been possible with simple explicit numerical schemes.

This method is not without a price in terms of computational complexity. Pressure can no longer be evaluated *directly* from the hydrostatic equation, because of an unknown reference pressure (e.g., pressure at the rigid lid can no longer be specified as atmospheric pressure), and is usually eliminated from the horizontal momentum equations by cross-differentiation. This raises the mathematical order of the equations and gives a Poisson boundary value problem to be solved at every time step for a stream function. The (mathematical) connectivity of the solution region becomes an important question in such problems for reasons of uniqueness. Introduction of a single island into a simple closed basin causes the solution region to become doubly connected, and makes the problem more difficult to solve. The multiple connectivity of the world ocean adds to difficulties of this sort. Nevertheless, long-term integrations have proved feasible by this method, at least for simple closed basins (Bryan and Cox 1968, Bryan 1969b, Cox 1970), and much has been learned from these solutions.

However, a slight inconsistency may arise when an ocean model filtered with the rigid lid approximation is coupled to an atmospheric model based on the unfiltered, primitive Eulerian equations (that is,

unfiltered in terms of external gravity waves). Most of the known atmospheric models are apparently of the unfiltered type. For these models, integrations spanning centuries would not be feasible with existing computers. Bryan (1969b) and Manabe (1969) have formulated a promising approach which may lead to fruitful investigations of long-term (order of centuries) changes in global climate. The essence of the method is that the atmospheric model is integrated for a relatively short period uniformly incremented over the course of the long-term integration of the oceanic counterpart. Some justification for this is found in the relatively rapid response of the atmosphere compared with that of the ocean.

Conversely, if jointly-running atmospheric and oceanic models are to simulate the same time span, then such times are apparently limited to several years, a decade perhaps, with present technology. This is in an equally important area of *seasonal* changes in climate. Of course a filtered ocean model can (and no doubt will) be used in such investigations. However, the need for larger time increments becomes less pressing, and the disadvantage of the filtered models may make the simplicity of the unfiltered models more appealing.

Thus, there appears to be a distinct need for an ocean model which may be simpler in concept and design, and which is intended only for simulations of from a few weeks duration to a few years.

This, then, is a resumption of the work begun by Crowley (1968) to construct a model of the stratified circulation of the world ocean based on the *unfiltered* primitive equations. Crowley's model may have been several years ahead of its time; a new generation of computers that allow minimal (spatially uniform) grid resolution of Gulf-Stream-type phenomena in the world ocean is only now becoming a reality. The present formulation will also take advantage of some simple concepts of conservation of quadratic quantities for nonlinear stability (although not in an exact sense in the present model), as discussed by Bryan (1966).

In many respects, with one notable exception, the formulation is a generalization of the homogeneous ocean model of Gates (1968). The exception is that, unlike Gates' model, the present model neglects

bottom topography. The purpose here is to approximate the thermally active circulation in only the upper few hundred meters of the ocean for seasonal simulations. The model, again like Crowley's, contains a horizontal bottom and vertical coastlines. But unlike Crowley's model, which contained six levels extending to 2000 m depth, the present model contains only two levels, and the total depth is 300 m. Inspiration, and some justification, for a two-level ocean model is found in the relative success achieved with simple two-level atmospheric models. Indeed, the plan, and hope, is to develop an ocean model that might be a true companion to the Rand version of the Mintz-Arakawa two-level atmospheric circulation model.

This report concentrates on formulation of the basic model for a bounded ocean basin, with application to the Pacific. Generalization to the world ocean, and coupling with the atmospheric counterpart, will be treated in separate publications.

II. PHYSICAL AND MATHEMATICAL MODEL

A. PHYSICAL MODEL

We wish to model the upper layers of the ocean in order to consider seasonal effects in the general circulation. Longer-term effects associated with the deeper circulation are neglected. Therefore, consider as a model a thermally stratified fluid which fills a shallow basin of uniform depth H on a rotating spherical earth. The fluid is bounded laterally by continental coastlines, assumed vertical. Coasts of islands likewise are assumed vertical. For definiteness, the depth H will be taken as 300 m, which corresponds roughly to the observed base of strong subsurface currents in equatorial regions (Knauss 1960).

In the simplest case, which is treated here, the fluid is thermally stratified, and salinity stratification is neglected. Again for definiteness, the flud is taken to be of uniform constant salinity, say $35^{o}/_{oo}$ (parts per thousand) for average sea water, and obeys a simple linear equation of state relating the density at atmospheric pressure to the temperature. This equation will be a linearization based on the formula proposed by Eckart (1958). Changes of phase will not be allowed in the model. Any sea ice present in high latitudes will be specified (from observation) in the model by arbitrarily setting the sea surface temperature equal to the (laboratory) freezing point of saline water of $35^{o}/_{oo}$ ($\sim -1.9^{o}C$).

The motion is driven by fluxes of heat and momentum across a free upper surface, and is retarded by turbulent frictional stresses at the coasts and possibly also at the bottom. All solid boundaries are assumed insulated and impermeable. The upper surface heat and momentum (wind stress) fluxes are specified climatologically as functions of position and of time. In general, the surface heat flux may include contributions proportional to the air-sea temperature difference, in which case the surface air temperature will be specified climatologically. Haney (1971b) has presented a simple and lucid formulation of a surface heat flux boundary condition for ocean circulation models. Formulation of the model directly in terms of heat fluxes as well as wind stresses may facilitate coupling the ocean model to its atmospheric counterpart.

One feature of the present model which may be open to serious question is the assumption of a horizontal bottom and abrupt, precipitous coastlines, i.e., the neglect of bottom topography. Evidence presented by Sarkisyan and Ivanov (1971) and others suggests that total (vertically integrated) transports can be significantly different in a stratified (or baroclinic) ocean with realistic bottom topography as opposed to a stratified ocean with a horizontal bottom. However, it is less clear how topography may affect *upper layer* transports in a stratified ocean. Nevertheless, one of several possible future improvements envisaged for the present model is to parameterize a nonvanishing vertical velocity at the lowermost level in the shallow ocean model, to partially account for topographic effects. In the interim, investigation of the simpler, horizontal-bottom model seems worthwhile.

Section VII further discusses the limitations of the model.

B. GOVERNING DIFFERENTIAL EQUATIONS

Large-scale ocean circulations are governed by the primitive Eulerian equations for an incompressible, inhomogeneous fluid. The momentum equations are in nearly complete form in the horizontal, but hydrostatic in the vertical, and the Boussinesq approximation is employed. The equations are written in a spherical coordinate system with λ and φ denoting longitude and latitude respectively. The vertical coordinate is z, taken positive upward from mean sea level. Undifferentiated factors $(a + z)^{-1} = (\text{radius})^{-1}$ in the flux-divergence terms are approximated by a^{-1}, where a is earth's mean radius. In vector notation and flux-divergence form, the equations are

$$\frac{\partial \underset{\sim}{v}}{\partial t} = \nabla \cdot (A_m \nabla \underset{\sim}{v} - \underset{\sim\sim}{vv}) + \frac{\partial}{\partial z} (\nu \frac{\partial \underset{\sim}{v}}{\partial z} - w\underset{\sim}{v})$$

$$- f\underset{\sim}{k} \times \underset{\sim}{v} - \frac{1}{\rho_\infty} \nabla p \qquad (2.1)$$

$$\frac{\partial p}{\partial z} = - \rho g \qquad (2.2)$$

$$\frac{\partial w}{\partial z} = - \nabla \cdot \underset{\sim}{v} \qquad (2.3)$$

$$\rho = \rho_\infty (1 - \alpha T) \tag{2.4}$$

$$\frac{\partial T}{\partial t} = \nabla \cdot (A_h \nabla T - \underset{\sim}{v} T) + \frac{\partial}{\partial z} (\kappa \frac{\partial T}{\partial z} - wT + q) \tag{2.5}$$

where $\underset{\sim}{v} = (u, v)$ is the horizontal velocity vector and ∇ the horizontal differential operator. The term $\nabla \cdot \underset{\sim\sim}{vv}$ in Eq. (2.1) denotes a vector having components $\nabla \cdot (\underset{\sim}{v}u)$ and $\nabla \cdot (\underset{\sim}{v}v)$. The gradient and divergence terms are defined by

$$\nabla( ) \equiv \frac{1}{a \cos \varphi} \frac{\partial( )}{\partial \lambda}, \frac{1}{a} \frac{\partial( )}{\partial \varphi}$$

$$\nabla \cdot \underset{\sim}{v}( ) \equiv \frac{1}{a \cos \varphi} \left\{ \frac{\partial u( )}{\partial \lambda} + \frac{\partial}{\partial \phi} [v( ) \cos \varphi] \right\}$$

$$\nabla^2( ) \equiv \frac{1}{a^2 \cos^2 \varphi} \frac{\partial^2( )}{\partial \lambda^2} + \frac{1}{a^2 \cos \varphi} \frac{\partial}{\partial \varphi} \left[\cos \varphi \frac{\partial( )}{\partial \varphi} \right].$$

The horizontal eddy coefficients of momentum, A_m, and heat, A_h, will be assumed constant. Thus, for instance, $\nabla \cdot A_m \nabla \underset{\sim}{v} = A_m \nabla^2 \underset{\sim}{v}$.

In Eq. (2.5) the heat flux term q is given by $S/\rho_\alpha c_p$, where S is short-wave radiation penetrating downward across the air-sea interface. This term will not be treated explicitly in the following; its contribution will be absorbed into the total surface heat flux Q_s, and vertical integrations will be taken over depths greater than those (~ 50 m) to which appreciable amounts of solar radiation can penetrate.

The horizontal bottom of the model ocean is placed at $z = -H$, and the upper surface is at $z = \zeta(\lambda, \varphi, t)$. It is assumed that $|\zeta| \ll H$. A vertical section of the model near a coastline is shown schematically in Fig. 1, in which amplitudes of ζ are grossly exaggerated, and in which certain other quantities appear that will be defined presently.

Boundary conditions for the model are as follows. At the air-sea interface, $z = \zeta(\lambda, \varphi, t)$:

$$\frac{\partial \zeta}{\partial t} + \underset{\sim}{v} \cdot \nabla \zeta = w_s(\lambda, \varphi, t) \tag{2.6}$$

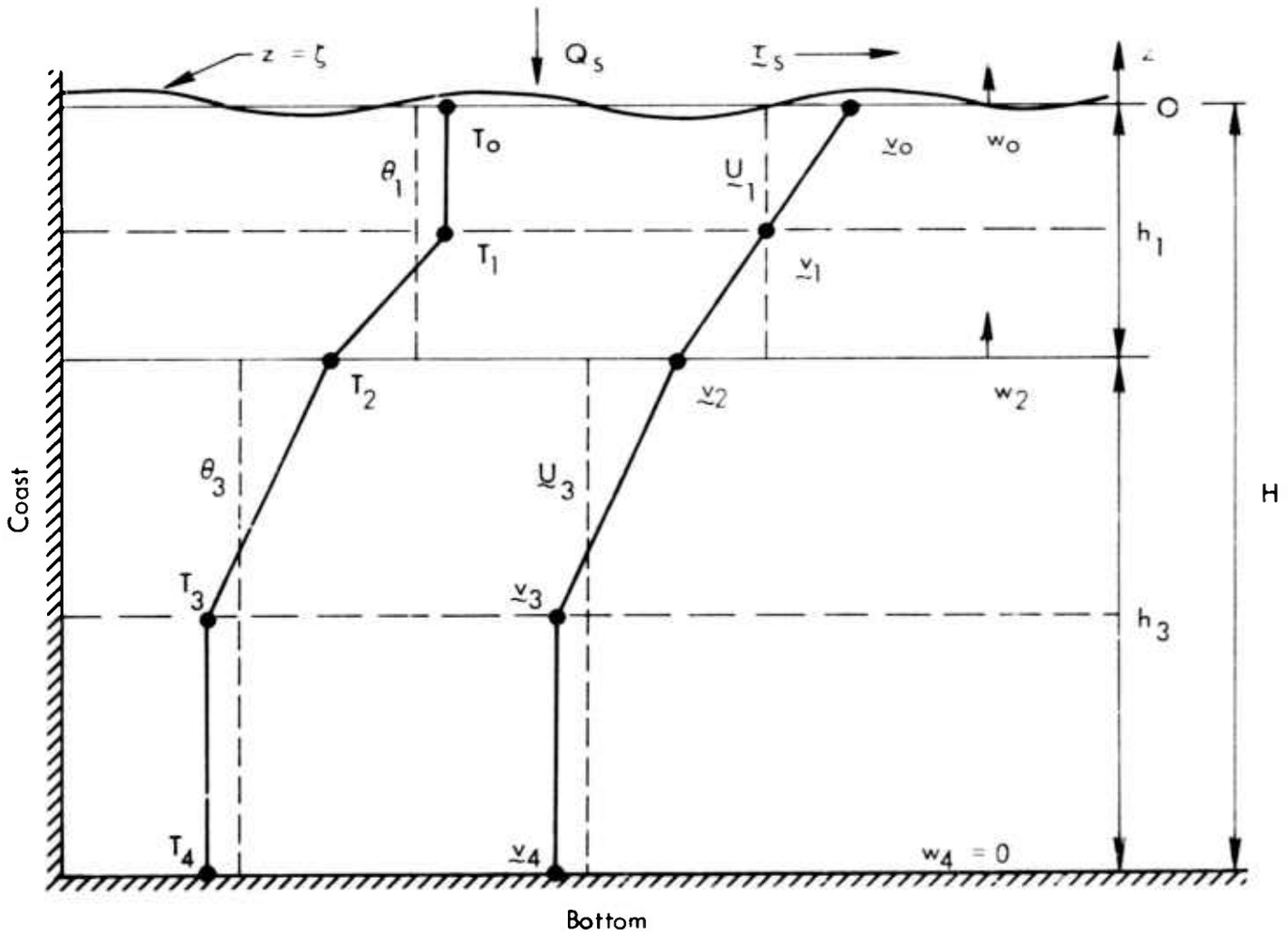

Fig. 1 — Schematic vertical section showing assumed distributions of temperature T and velocity $\underset{\sim}{v} = (u, v)$. Layer 1 (upper) is bounded by levels 0 and 2, layer 3 (lower) by levels 2 and 4. θ_k is the average T for layer k = 1, 3. Similarly, $\underset{\sim}{U}_k$ is the average $\underset{\sim}{v}$.

$$\nu \frac{\partial \underset{\sim}{v}}{\partial z} = \frac{1}{\rho_\infty} \underset{\sim}{\tau}_s(\lambda, \varphi, t) \tag{2.7}$$

$$\kappa \frac{\partial T}{\partial z} + q = \frac{1}{\rho_\infty c_p} Q_s(\lambda, \varphi, t) \tag{2.8}$$

where $\underset{\sim}{\tau}_s$ is the horizontal wind stress vector and Q_s is the total vertical heat flux across the air-sea interface. Equations (2.7) and (2.8) represent a slight approximation consistent with the hydrostatic form of the governing equations. In a more general formulation, Eq. (2.7), for instance, would equate the normal derivative of the *tangential* (as opposed to horizontal) component of velocity evaluated at $z = \zeta$ to the *tangential* component of wind stress. This expression hardly differs from that given above if sea surface slopes are small.

At the bottom, $z = -H$:

$$w = 0 \tag{2.9}$$

$$\nu \frac{\partial \underset{\sim}{v}}{\partial z} = \frac{1}{\rho_\infty} \underset{\sim}{\tau}_b \tag{2.10}$$

$$\frac{\partial T}{\partial z} = q = 0 \tag{2.11}$$

where an assumption is required to relate the bottom stress $\underset{\sim}{\tau}_b$ to the velocity field. The simplest assumption consistent with Fig. 1 is that $\underset{\sim}{\tau}_b = 0$. A slightly more general formulation, which is used in the model, assumes that the bottom stress is proportional to the average velocity in the lower layer. The "friction" coefficient of proportionality may then be set equal to zero to give the simpler, no-stress case.

Conditions at the coasts are

$$\underset{\sim}{v} = (\text{normal component of } \nabla T) = 0 \tag{2.12}$$

Integration of the continuity Eq. (2.3) between the bottom and the sea surface, and application of the boundary conditions (2.6) and (2.9) gives the first of the following two equations:

$$\frac{\partial \zeta}{\partial t} = - \nabla \cdot \int_{-H}^{\zeta} \underset{\sim}{v} dz \tag{2.13}$$

$$p = p_a + \rho_\infty g \left[\zeta - z - \alpha \int_z^\zeta T(z')dz' \right] \tag{2.14}$$

Leibnitz's rule was employed to combine the integrated divergence with the advection term in arriving at (2.13). The pressure Eq. (2.14) is obtained by combining (2.2) and (2.4) and integrating between a (variable) level z and the sea surface where p_a is atmospheric pressure.

There appears to be no exact energy integral for the foregoing system of governing equations when the fluid has a free surface. This difficulty is not encountered in models in which all boundaries are rigid, because the processes of time-differentiation and integration over a fixed volume can be freely interchanged. The difficulty arises here principally because of an ambiguity in the definition of density, ρ versus ρ_∞. Stated another way, the Boussinesq approximation should be applied *after* the more exact expression for energy is derived. Thus, if ρ_∞ is replaced with ρ in Eq. (2.1) and energy is derived in the usual way except that integration is over the entire *mass* of fluid (as opposed to volume integration), then the order of time-differentiation and integration can be interchanged. There results:

$$\frac{d}{dt}(K + P) = - \int_{\text{sea surface}} \int p_a \underset{\sim}{v}_3 \cdot \underset{\sim}{n} d\sigma + \overline{W} + \overline{Q}$$

where

$$K = \iiint \frac{1}{2} \rho \underset{\sim}{v}^2 dxdydz \tag{2.15}$$

$$P = \iiint \rho g z dxdydz \tag{2.16}$$

Here, the mass integrals have been changed back to volume integrals by the transformation d(mass) = ρdxdydz. $\overline{W}$ represents the volume integral of the work done by the eddy diffusion terms in (2.1), $\overline{Q}$ the heating done by the eddy conduction terms and the source q in (2.5). The surface integral represents the work done by atmospheric pressure, where $\underset{\sim}{v}_3$ is the three-dimensional velocity vector and $\underset{\sim}{n}$ the unit outward normal to the sea surface. The above has the usual integral K + P = const in the absence of eddy diffusion processes, sources of heat, and work done by atmospheric pressure.

Consistent with the Boussinesq approximation, ρ is now approximated by ρ_∞ in the kinetic energy (2.15) but is retained in its more complete form in (2.16).

To this point no additional approximations have been introduced beyond those implicit in the hydrostatic and Boussinesq form of the governing equations. The foregoing, except for Eq. (2.13), is similar to the system of equations used by Crowley (1968), to which the reader may wish to refer for a derivation from the more complete three-dimensional equations in a spherical coordinate system. Use of Eq. (2.13) for predicting surface elevation was pointed out by Gates (1968).

The foregoing is to be solved numerically as an initial value problem. For given initial distributions of temperature, velocity, and surface elevation, predictions of these same quantities are to be made subject to the boundary conditions, including prescribed sea-surface distributions of heating and wind stress. Evaluations of total energy during the course of the integration provide a measure of the stability of the solution, and of the approach to a steady state.

III. FINITE DIFFERENCE EQUATIONS

A. APPROXIMATED LAYER EQUATIONS: VERTICAL DIFFERENCING

Vertical differencing requires special care for several reasons, and is therefore treated separately. One principal reason is the hydrostatic assumption relating to the vertical coordinate. Another is the relative crudeness of resolution of a model possessing only two levels in the vertical. Some care is required to justify what may appear to be rather overly detailed vertical distributions of the dependent variables in a two-level model. The approach is by means of vertical integration. However, the results will be formally the same as differential/vertical-difference equations.

We approximate, first by retaining the surface elevation ζ only to lowest order in Eqs. (2.13) and (2.14). The upper limits of integration are replaced with zeros, and the resulting system of equations is treated as if the upper surface were horizontal. In (2.13) this amounts to neglecting the divergence in the layer of thickness $|\zeta|$ compared with the divergence in the much larger layer of constant thickness H. (The sign of the contribution is changed for $\zeta < 0$.) The approximation will permit interchanging the order of differentiation and integration, and all resulting variables except the nonlinear advections can be written directly in terms of their integrated averages.

Secondly, in the horizontal advection terms we will approximate the average of products with the product of averages, e.g., $\overline{\underset{\sim}{v}T} \simeq \overline{\underset{\sim}{v}}\,\overline{T}$. This approximation, although common in numerical schemes, is more difficult to justify, especially in a crude two-level model. Some justification is found in the quadratic-conserving (and hence stabilizing) properties of the numerical scheme when simple averages of variables are used. The approach used here in treating the advection terms is described by Bryan (1966).

Define two layers of constant thickness h_1 (layer 1) and h_3 (layer 3) as shown in Fig. 1. Layer 1 is bounded by level 0 (mean sea level) and the intermediate level 2; layer 3 is between level 2 and level 4 at the horizontal bottom. Vertically averaged values of $\underset{\sim}{v}$ and T for

layer k (k = 1, 3) are denoted by $\underset{\sim}{U}_k$ and θ_k as shown in Fig. 1, and are defined for layers of constant thickness, e.g.,

$$\underset{\sim}{U}_k = \frac{1}{h_k} \int_{k+1}^{k-1} \underset{\sim}{v} dz$$

for k = 1 and 3, where the limits k ± 1 denote constant z-levels bearing those subscripts, and where h_k is constant. The vertically averaged pressure is denoted by π_k.

With these definitions and approximations, the governing momentum, heat, and continuity equations, vertically integrated over layer k, take the following form:

$$\frac{\partial \underset{\sim}{U}_k}{\partial t} = \nabla \cdot \left(A_m \nabla \underset{\sim}{U}_k - \underset{\sim}{U}_k \underset{\sim}{U}_k \right) + \frac{1}{\rho_\infty h_k} \left(\underset{\sim}{\tau}^*_{k-1} - \underset{\sim}{\tau}^*_{k+1} \right)$$

$$- f \underset{\sim}{k} \times \underset{\sim}{U}_k - \frac{1}{\rho_\infty} \nabla \pi_k \qquad (3.1)$$

$$\frac{\partial \theta_k}{\partial t} = \nabla \cdot \left(A_h \nabla \theta_k - \underset{\sim}{U}_k \theta_k \right) + \frac{1}{\rho_\infty c_p h_k} \left(Q^*_{k-1} - Q^*_{k+1} \right) \qquad (3.2)$$

$$w_{k-1} - w_{k+1} = h_k \nabla \cdot \underset{\sim}{U}_k \qquad (3.3)$$

where $\underset{\sim}{\tau}^*$ and Q^* are *total* vertical transfer terms defined by

$$\frac{1}{\rho_\infty} \underset{\sim}{\tau}^*_{k-1} = \left(\nu \frac{\partial \underset{\sim}{v}}{\partial z} - w \underset{\sim}{v} \right)_{k-1} \qquad (3.4)$$

$$\frac{1}{\rho_\infty c_p} Q^*_{k-1} = \left(\kappa \frac{\partial T}{\partial z} - wT + q \right)_{k-1} \qquad (3.5)$$

The right sides of Eqs. (3.4) and (3.5) are evaluated at levels 0, 2, and 4. The advective fluxes are absent in the sea-surface boundary conditions (2.7) and (2.8) because there is no advective flux (in a

Lagrangian sense) across a fluid material surface. In the present approximation, surface conditions are applied at mean sea level, and continuity of fluxes of momentum and heat means that vertical advections must be included. In place of Eqs. (2.7) and (2.8) we have

$$\underset{\sim}{\tau}_0^* = \underset{\sim}{\tau}_s(\lambda, \varphi, t) \tag{3.6}$$

$$Q_0^* = Q_s(\lambda, \varphi, t) \tag{3.7}$$

No modification is required at the bottom, where Eqs. (2.9) through (2.11) give $\underset{\sim}{\tau}_4^* = \underset{\sim}{\tau}_b$ and $Q_4^* = 0$. Formulated in the model is the assumption

$$\underset{\sim}{\tau}_b = K\underset{\sim}{U}_3 \tag{3.8}$$

where K is a constant bottom-friction coefficient.

Evaluation of Eqs. (3.4) and (3.5) at the intermediate level 2 requires additional assumptions. For the advection terms, w_2 is evaluated from (3.3), and $\underset{\sim}{v}_2$ and T_2 are assumed to be simple two-point averages of the form

$$T_2 = \frac{1}{2}(\theta_1 + \theta_3) \tag{3.9}$$

with a similar expression relating $\underset{\sim}{v}_2$ to $\underset{\sim}{U}_1$ and $\underset{\sim}{U}_3$. (See Fig. 1.)

The above choice is inspired by conservation of quadratic quantities, and hence stability of the numerical scheme, although not in an exact sense for a (divergent) model with a free upper surface. Assuming comparable treatment of the horizontal finite differencing, the square of a scalar such as T is conserved in the sense of Bryan (1966) if averages of the form of (3.9) are used, *provided also* that the normal component of velocity is zero at all boundaries. Conservation of T^2, U^2, and V^2 is only approximate in the present model because the vertical velocity is not zero at the upper "boundary" at mean sea level. Thus, for example,

$$\frac{d}{dt}\iiint T^2 dxdydz = -\iint_{\substack{\text{mean sea}\\ \text{level}}} wT^2 d\sigma$$

where volume integration is over the entire space-fixed volume bounded above by mean sea level. Conservation of T, U, and V, and their squares, in the present model is in the more limited sense that the usual conservation would hold if the vertical velocity were zero at the uppermost level.

The vertical derivatives in Eqs. (3.4) and (3.5) are evaluated as the average of the respective derivatives occurring just above and just below level 2. This requires assumptions on the more detailed vertical distributions of $\underset{\sim}{v}$ and T. Assumed in the model are the piecewise-linear distributions shown in Fig. 1. The temperature T_0 is set equal to T_1 as a crude representation of the observed mixed upper layer in the oceans. T_4 is set equal to T_3 to be consistent with zero conduction into the bottom. The temperature derivative at level 2 is

$$\left(\frac{\partial T}{\partial z}\right)_2 = \frac{T_1 - T_2}{h_1} + \frac{T_2 - T_3}{h_3} \tag{3.10}$$

in which T_2 is given by Eq. (3.9). With the assumed vertical distribution, the other temperatures can be related to the averages. One finds

$$T_1 = \frac{1}{6}(7\theta_1 - \theta_3) \tag{3.11}$$

$$T_3 = \frac{1}{6}(7\theta_3 - \theta_1) \tag{3.12}$$

As stated previously, h_1 is assumed greater than the depth of penetration of appreciable solar radiation. Therefore, q = 0 at level 2. This completes the specification of Eq. (3.5) for the vertical differencing.

For the velocity it does not seem clear that a "mixed layer" of velocity would necessarily be appropriate. (Velocities in the general

circulation are not readily subject to direct measurement except in regions of strong and persistent currents.) Implicit in the model is the assumption that h_1 is much larger than the thickness of the upper frictional layer. Therefore, Ekman-layer dynamics are not resolved by the model. Perhaps the simplest assumption, and the one used here, is to let $\underset{\sim}{v}_0$ be a linear extrapolation from $\underset{\sim}{v}_1$ and $\underset{\sim}{v}_2$. (This assumption can be easily modified in the model.) Again, $\underset{\sim}{v}_4$ is set equal to $\underset{\sim}{v}_3$ to model a no-stress distribution in the lowermost portion, and an equation of the form of (3.10) is assumed for the velocity derivative at level 2. The velocity $\underset{\sim}{v}_2$ is again a two-point average of the form of (3.9), and one finds

$$\underset{\sim}{v}_1 = \underset{\sim}{U}_1 \tag{3.13}$$

$$\underset{\sim}{v}_3 = \frac{1}{6}\,(7\underset{\sim}{U}_3 - \underset{\sim}{U}_1) \tag{3.14}$$

This completes the specification of (3.4) for the vertical differencing.

The layer equations are completed with the following, the first two of which are the approximations of Eqs. (2.13) and (2.14) when the upper limits of integration are replaced with zero.

$$\frac{\partial \zeta}{\partial t} = -\nabla \cdot (h_1\underset{\sim}{U}_1 + h_3\underset{\sim}{U}_3) = -h_1 \nabla \cdot \underset{\sim}{U} - h_3 \nabla \cdot \underset{\sim}{U}_3 \tag{3.15}$$

$$\pi_1 = p_a + \rho_\infty g \left[\zeta - \frac{\alpha h_1}{18}\,(8\theta_1 + \theta_3)\right] \tag{3.16}$$

$$\pi_3 = \pi_1 - \frac{1}{4}\,\rho_\infty g \alpha H(\theta_1 + \theta_3) \tag{3.17}$$

The above-mentioned first-order approximation is seen to amount to a linearization. Equation (3.15), together with the continuity equation and the condition $w_4 = 0$, give $\partial\zeta/\partial t = w_0$, which is a linearization of (2.6).

Equation (3.16) is the vertical average of (2.14) over layer 1, in which the upper limit of integration ζ is replaced with zero. The

dynamically unimportant term $\rho_\infty gz$ integrates to a constant, which is omitted. The first two terms on the right of (3.16) are the contributions to pressure which can occur in the simple case of a homogeneous fluid. Of these, the term p_a is probably negligible in most simulations of the general circulation (see Gates 1966) but is retained here for slightly greater generality. The last terms are the baroclinic contributions to pressure. The particular form, e.g., the rational factor 8/18, resulted from the assumed piecewise-linear distribution of temperature. For reasonable values of temperature, the baroclinic part of (3.16) is nearly equal to $-\frac{1}{2}\rho_\infty g\alpha h_1\theta_1$, which would have resulted if temperature had been assumed vertically uniform in the top layer.

Equation (3.17) did not result from vertical integration of (2.14) but, rather, is inspired by (approximate) conservation of total energy. Equation (3.17) can be rewritten as

$$\frac{\pi_1 - \pi_3}{\frac{1}{2}h_1 + \frac{1}{2}h_3} = \rho_\infty g\alpha T_2 \tag{3.18}$$

which is a finite-difference approximation to the hydrostatic equation evaluated at level 2. It can be shown (e.g., Haney 1971a) that Eq. (3.18) represents one of several (sufficient) conditions on the ensuing numerical scheme to conserve total energy if the vertical velocity were zero at mean sea level.

B. HORIZONTAL AND TIME DIFFERENCING

The foregoing system of equations is written in finite difference form on a horizontally staggered grid. The grid is similar to that used by Bryan (1969a) and others, except possibly for the location of coastal boundaries. The basic unit, shown in Fig. 2, for constructing the grid consists of two temperature elements stacked one over the other. Average temperatures are stored at the center of each of the two elements. The average velocities are stored at the corners of the elements at the same levels as the temperatures. Surface elevation, which is independent of depth, is stored at a horizontal position coincident with the temperature points. Vertical velocities (not shown)

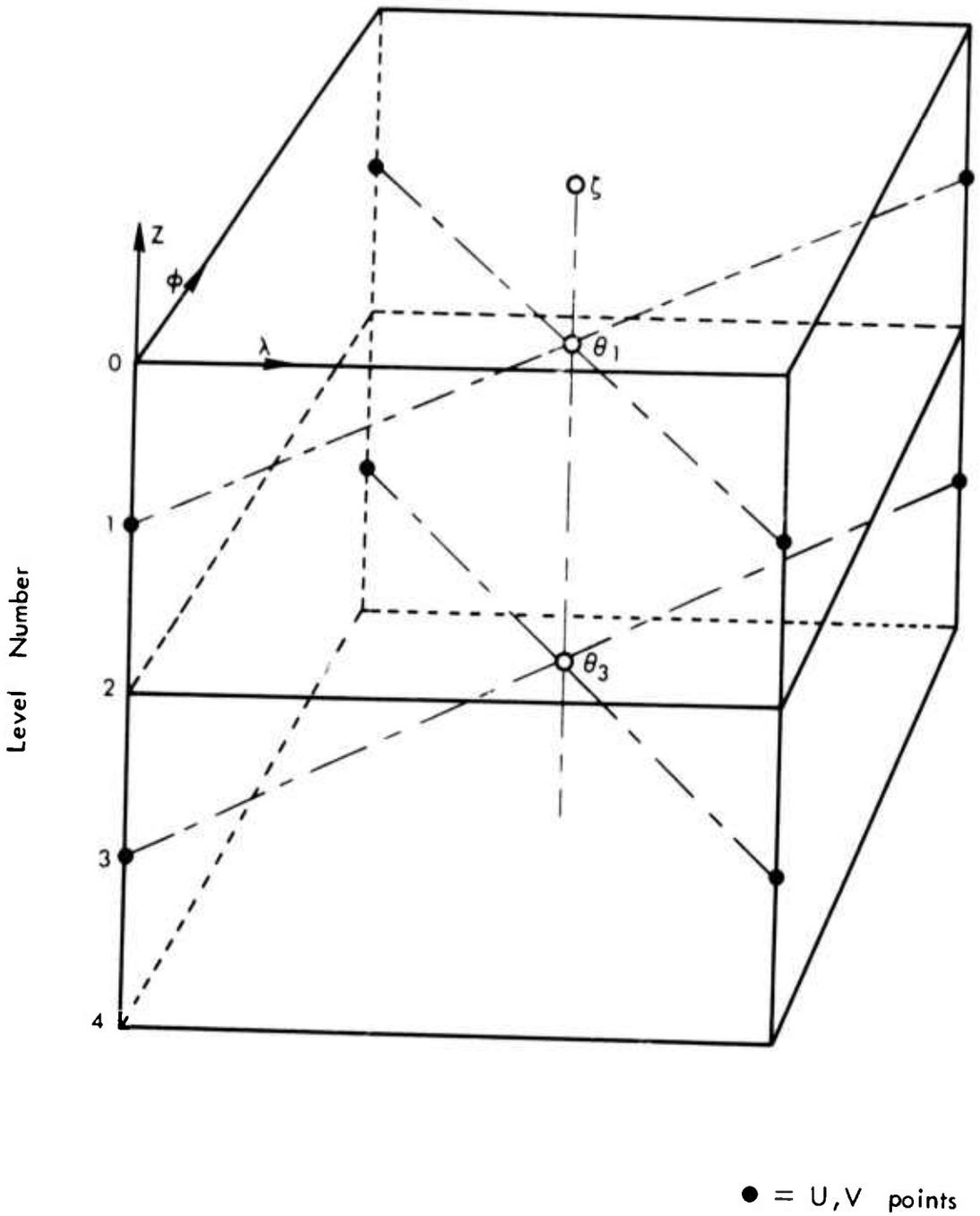

Fig. 2— Schematic representation of two temperoture box elements stocked one over the other. This double element is the basic building block of the two-level ocean model. Averoge temperotures θ_k, shown in Fig. 1, ore stored ot the center of eoch element on levels 1 ond 3. Average velocities $\underset{\sim}{U}_k$ ore stored ot the corners of the boxes. Layer thicknesses ore shown equol to each other for clority.

are evaluated diagnostically at levels 2 and 0. As described below, this is done separately for U, V points and for ζ, θ points.

The grid is regular in a spherical coordinate system, i.e., $\Delta\lambda$ and $\Delta\varphi$ are chosen constant. The east-west distance between adjacent velocity points, and between adjacent temperature points, is $a \cos \varphi \, \Delta\lambda$, which decreases toward the poles. The respective north-south dimensions are uniformly $a\Delta\varphi$.

Horizontal velocities are stored at integer-index values of latitude and longitude, in which indices are counted positive eastward and northward with respect to reference values λ_1, φ_1, located at the extreme southwest corner:

$$\lambda_i = \lambda_1 + (i - 1)\Delta\lambda, \qquad i = 1, 2, \ldots, M + 1$$

$$\varphi_j = \varphi_1 + (j - 1)\Delta\varphi, \qquad j = 1, 2, \ldots, N + 1$$

The temperatures and surface elevation are stored at half-integer index locations given by

$$\lambda_{i\pm\frac{1}{2}} = \lambda_i \pm \frac{1}{2}\Delta\lambda$$

$$\varphi_{j\pm\frac{1}{2}} = \varphi_j \pm \frac{1}{2}\Delta\varphi$$

In general there are $(M + 1) \times (N + 1) \times 2$ velocity points and $M \times N \times 2$ temperature points, or, equivalently, $M \times N$ of the double elements of Fig. 2. Some elements will denote artificial land points, to be discussed presently.

The simplest case of a rectangular basin is shown schematically in Fig. 3. Indicated there by the dashed lines is a typical double element for temperature as viewed from above. The basin in this case is bounded by single rows and columns of artificial temperature elements.

The following standard notation is adopted for divided differences and two-point averages:

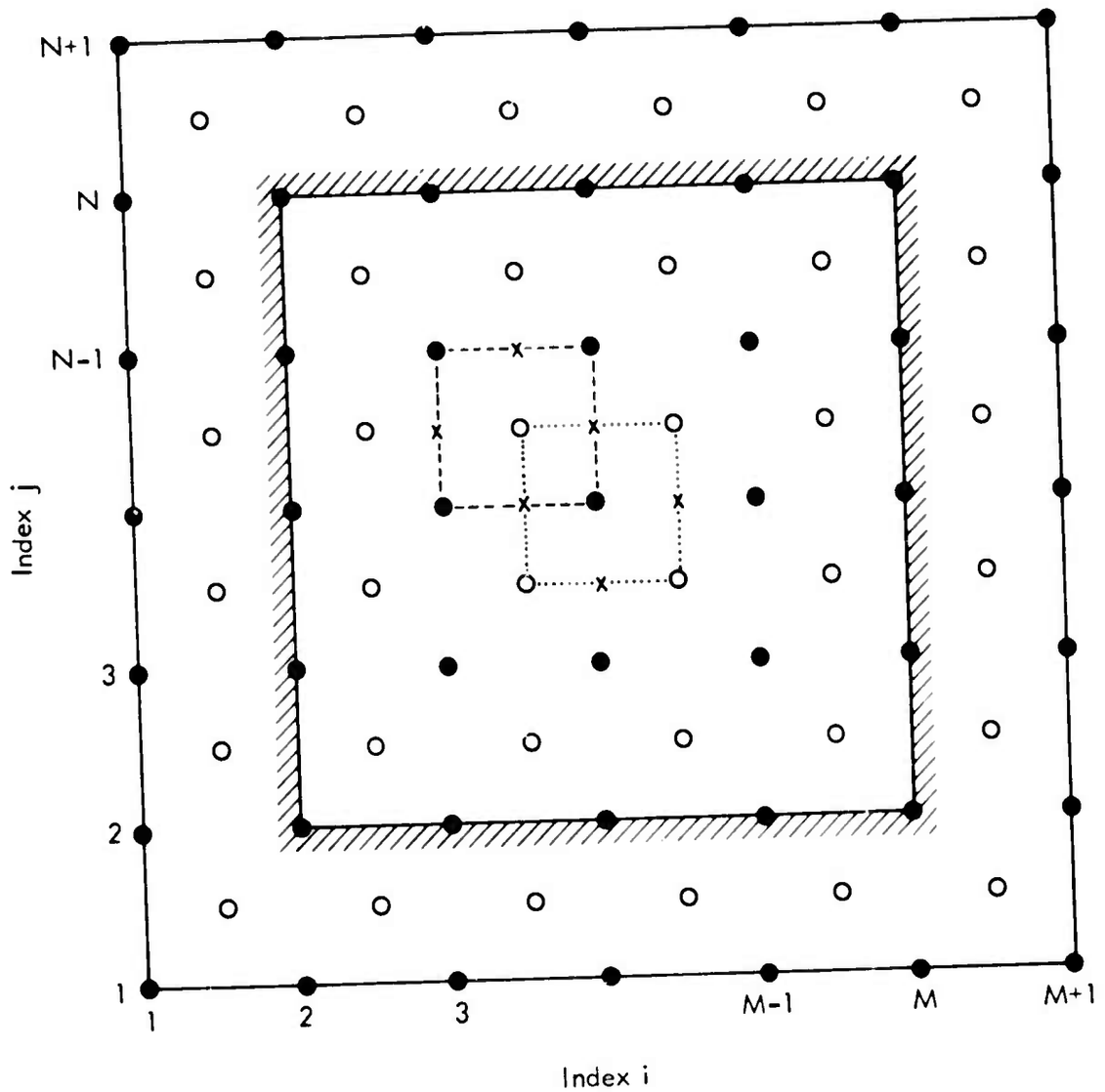

Fig. 3— Layout of the horizontal grid composed of M x N of the double elements of Fig. 2. Shown is the simple case of a rectangular basin bounded by artificial land elements. A typical temperature element of Fig. 2 is denoted by the dashed lines, a typical velocity element by the dotted lines. Average velocities used in calculating advective fluxes are evaluated at points denoted by x.

$$\delta_\lambda \theta(\lambda) = \frac{\theta\left(\lambda + \frac{1}{2}\Delta\lambda\right) - \theta\left(\lambda - \frac{1}{2}\Delta\lambda\right)}{\Delta\lambda}$$

$$\overline{\theta(\lambda)}^{\lambda} = \frac{1}{2}\left[\theta\left(\lambda + \frac{1}{2}\Delta\lambda\right) + \theta\left(\lambda - \frac{1}{2}\Delta\lambda\right)\right]$$

with similar expressions with respect to latitude and time. Thus, for instance, a central difference in time evaluated at time t with increment $2\Delta t$ is $\delta_t \overline{\theta(t)}^t$. A similar notation is used for vertical divided differences and averages; however, a subscript k is used to distinguish between the upper and lower elements of Fig. 2. For instance,

$$\delta_z w_k = \frac{w\left(z_k + \frac{1}{2}h_k\right) - w\left(z_k - \frac{1}{2}h_k\right)}{h_k} = \frac{w_{k-1} - w_{k+1}}{h_k}$$

in which k assumes the values 1 and 3.

The Laplacian in finite difference form will be the same when applied to both temperature and velocity:

$$\Delta^2\theta = \frac{1}{a^2 \cos\varphi}\left[\frac{1}{\cos\varphi}\delta_\lambda\delta_\lambda\theta + \delta_\varphi(\cos\varphi\,\delta_\varphi\theta)\right]$$

These quantities require no averaging of the dependent variables at intermediate points, whereas the advections will require averaging.

The advection operator used at temperature points differs from that used at velocity points. Equations (3.2), (3.3), and (3.15) applied to the elements of Fig. 2 are given the following finite difference forms:

$$\delta_t \overline{\theta}^t_k = A_h \Delta^2\theta_k - \nabla_a \cdot (\underset{\sim}{U}\theta)_k + \frac{1}{\rho_\infty c_p}\delta_z Q^*_k \tag{3.19}$$

$$\delta_z w_k = -\nabla_a \cdot \underset{\sim}{U}_k \tag{3.20}$$

$$\delta_t \overline{\zeta}^t = - h_1 \nabla_a \cdot \underset{\sim}{U}_1 - h_3 \nabla_a \cdot \underset{\sim}{U}_3 = w_0(t) \tag{3.21}$$

where

$$\nabla_a \cdot (\underset{\sim}{U}\theta)_k = \frac{1}{a \cos \varphi} \left[\delta_\lambda (\overline{U}^{\varphi} \overline{\theta}^{\lambda}) + \delta_\varphi (\cos \varphi \overline{V}^{\lambda} \overline{\theta}^{\varphi}) \right]_k \tag{3.22}$$

and where $\nabla_a \cdot \underset{\sim}{U}_k$ is obtained from (3.22) by setting $\theta \equiv 1$ in the latter.

The form of (3.22) is quadratic-conserving in the sense of Bryan (1966). The horizontal fluxes of θ and of θ^2 across vertical faces of all temperature elements are equal and opposite. For instance, the eastward flux of θ across each of the easternmost faces of the double element shown in Fig. 2 involves the product of $\overline{U}^{\varphi}$, which is the north-south average of the eastward velocities at the northeast and southeast corners, and $\overline{\theta}^{\lambda}$, which is the east-west average of the respective temperatures of the element shown and those of the element immediately to the east. This flux is exactly equal (but of opposite sign) to that entering the western face of the neighboring element as evaluated by (3.22). For the vertical advective fluxes the quantity Q_2^* in Eq. (3.19) contains the term $w_2 T_2 = w_2(\theta_1 + \theta_3)/2$, where w_2 is evaluated from (3.20). The vertical advective flux between the two elements is again equal but of opposite sign, and cancels out in the summation process.

A corresponding set of equations, but with a different advection operator, is applied to all interior velocity points. A typical velocity element viewed from above is indicated by the dotted lines in Fig. 3. Such elements are similar to that shown in Fig. 2 except that $\underset{\sim}{U}_1$ and $\underset{\sim}{U}_3$ are situated along the center line and ζ, θ_1, and θ_3 are at the corners. Equations (3.1) and (3.3) are applied to these elements in the following finite difference form:

$$\delta_t \overline{\underset{\sim}{U}_k}^t = - \nabla_b \cdot (\underset{\sim\sim}{UU})_k + A_m \Delta^2 \underset{\sim}{U}_k + \frac{i}{\rho_\infty} \delta_z \underset{\sim}{\tau}_k^*$$

$$- f_k \underset{\sim}{k} \times \underset{\sim}{U}_k - \frac{1}{\rho_\infty a} \left(\frac{1}{\cos \varphi} \delta_\lambda \overline{\pi_k}^{\varphi}, \delta_\varphi \overline{\pi_k}^{\lambda} \right) \tag{3.23}$$

$$\delta_z w_k = - \nabla_b \cdot \underset{\sim}{U}_k \tag{3.24}$$

where

$$\nabla_b \cdot (\underset{\sim\sim}{UU})_k = \frac{1}{a \cos \varphi} \left\{ \delta_\lambda (\overline{U}^\lambda \overline{\underset{\sim}{U}}^\lambda) + \delta_\varphi [\overline{(\cos \varphi V)}^\varphi \overline{\underset{\sim}{U}}^\varphi] \right\}_k \tag{3.25}$$

and where $\nabla_b \cdot \underset{\sim}{U}_k$ is obtained from Eq. (3.25) by replacing the *vector* quantities $\overline{\underset{\sim}{U}}^\lambda$ and $\overline{\underset{\sim}{U}}^\varphi$ on the right side with one. The pressure differences in Eq. (3.23) are evaluated using (3.16) and (3.17).

The advection operator ∇_b is quadratic conserving in U_k and V_k. Again, the vertical advection is $w_2 \underset{\sim}{v}_2 = w_2 (\underset{\sim}{U}_1 + \underset{\sim}{U}_3)/2$, which is contained in the term $\underset{\sim}{\tau}_2^*$ of (3.23), and is of a quadratic conserving form. Here, w_2 is calculated from (3.24) instead of (3.20).

At the beginning of an integration, and for subsequent restarts, a single forward time difference is used in place of the central time differences in Eqs. (3.19), (3.21), and (3.23). Central time differences are used for the remainder except that the diffusion terms are lagged one time step for stability.

IV. GENERAL GRID SETUP AND BOUNDARY CONDITIONS

A. TREATMENT OF IRREGULAR BOUNDARIES

The basic idea is to fill all water regions of an ocean basin with the temperature double-elements of Fig. 2 in such a way that velocity points lie on the boundaries. The (horizontal) velocities are held identically zero there. Land regions are filled with similar but artificial elements which, except for land-coastal points, are never used in the calculations. At all land-coastal points, i.e., temperature-box elements immediately adjacent to water regions, the values of temperature are adjusted to satisfy the insulating condition at coasts (meaning zero conduction there because horizontal advections are zero from the velocity condition). The approach appears similar to that used in the Indian Ocean model of Cox (1970).

The insulating condition is satisfied approximately in the present model by setting land-coastal values of temperature equal to the average of values for adjacent sea-coastal points. This is done initially and at the end of every subsequent time step. The method is indicated in Fig. 4 for the case of an island. The temperatures θ_1 and θ_3 at the land point labeled 8 are set equal to the corresponding temperatures at the sea point immediately to the left, which, in this case, exactly satisfies the insulating condition. However, the temperatures at the land point labeled 9 + 1 are set equal to the averages (θ_1 and θ_3 respectively) of the temperatures at sea-points labeled 9 and 1, which is only an approximation to the insulating condition. An extreme case is that of an island consisting of a single element for which the temperatures θ_1 and θ_3 are the respective averages of those for the four adjacent sea points. Outer lateral boundaries of the bounded basin, not shown in Fig. 2, are treated in a similar fashion.

It is also possible to formulate the model so as to satisfy exactly the insulating condition at coast lines, but the method is more complex than seems justified in a model that neglects continental shelf topography. In the exact method a significant number of land-coastal temperatures would have to be changed twice (some as many as four times)

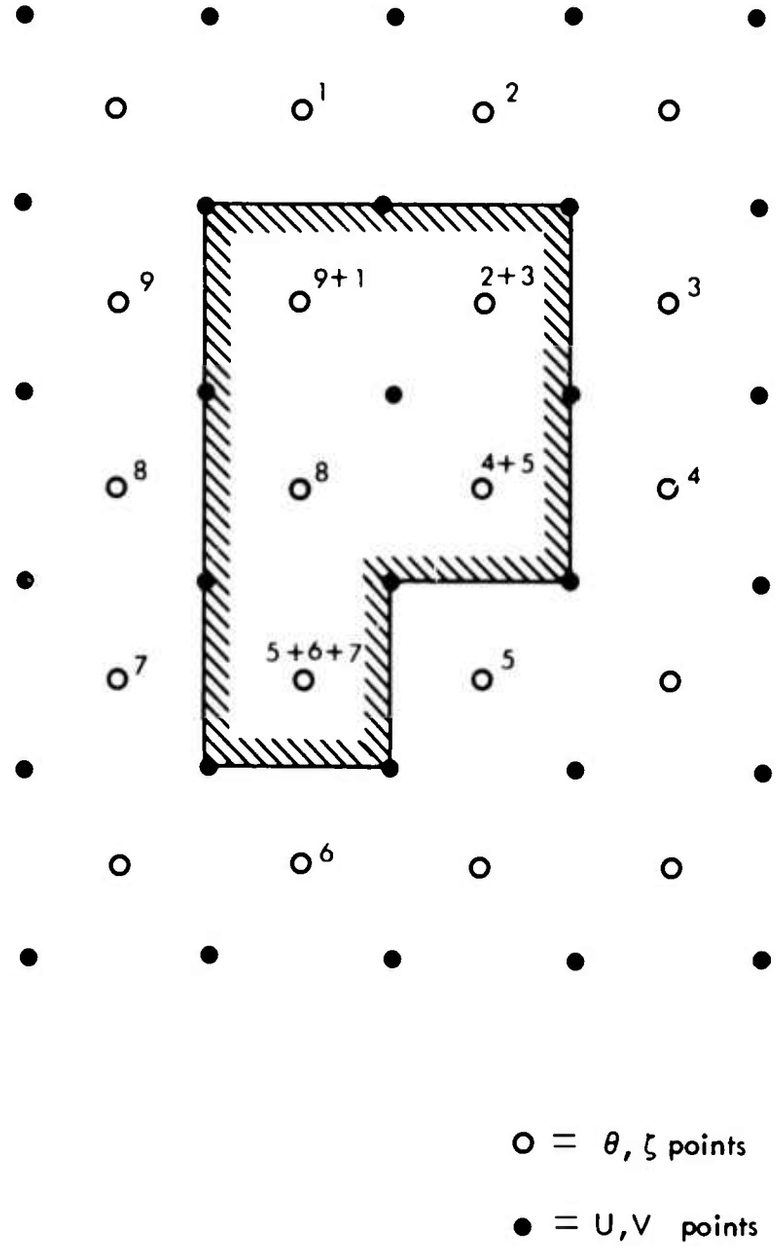

Fig. 4 — Schematic indicating the method used in constructing the more general grid and in satisfying lateral boundary conditions for irregular geometries. The ocean is filled with the temperature elements of Fig. 2. Adjacent land areas (e.g., the island shown) are filled with similar but artificial elements. Velocities U, V are maintained identically zero within all land areas and on the boundaries. Insulating conditions at coastlines are satisfied approximately by setting land-coastal values of temperature equal to the average of values for adjacent sea-coastal points. See text for explanation of numbers.

during the calculations for each time step. In any event, the boundaries for real ocean circulations are not well defined here and are not precisely insulated. (In the case of the Pacific model reported on below, the "boundaries" were placed at the 100-m depth contour.) On balance, the approximate method appears better because of its simplicity.

B. THE GEOGRAPHY ARRAY

The general treatment of boundary conditions is perhaps best described in terms of the geography array which is input to the model. This is an M × N array corresponding to the total number of temperature double-elements of Fig. 2 (cf. the simple M × N array of Fig. 3). Each element of the input array contains one of three simple pieces of information: zero (blank) if it is a regular sea point, "I" if it is a sea point covered by sea ice, or "L" if it is a land point. The program then processes this information and sets up a slightly more elaborate M × N array which controls the treatment of each point at every time step. The initial setup goes somewhat as follows.

For all land points the associated velocities, eight for each element shown in Fig. 2, are set to zero and tagged so that they are never changed during the course of the integration. Land-temperature points away from the coast are similarly tagged and never used in the calculations. All land-coastal points are given a special number, stored in the geography array, according to the type of point. This number tells the program how to do the temperature-averaging, initially and at the end of each time step. For instance, all land-coastal points such as the one labeled 2 + 3 in Fig. 4 are given the same identifying number. After every time step the temperatures at all such 2 + 3 points are set equal to the averages of the respective temperatures at the sea-points immediately to the east and to the north.

All sea-ice points retain a single identifying number and are treated the same way. The temperatures at both levels are set and held fixed at $-1.9^{\circ}C$, roughly the (laboratory) equilibrium temperature of ice and saline water of $35^{\circ}/_{oo}$ salinity. The temperature prediction equation is ignored at these points, as is the (input) surface heat flux Q_s. However, the surface wind stress $\underset{\sim}{\tau}_s$ together with Eqs. (3.23)

and (3.24) are used to predict the velocities at these points. Sea ice is an exceedingly inhomogeneous and anisotropic substance containing numerous cracks and leads, and is in nearly constant motion from surface winds. The model represents sea ice as a massless, completely extensible and compressible membrane through which wind stress is transmitted without attenuation to the nearly homogeneous water below. This is probably one of the cruder features of the model.

Finally, if the geography array indicates a regular sea point, the complete set of prediction equations is employed, including (input) surface heating and wind stress. All sea points adjacent to land, both velocity and temperature points, are treated just like the corresponding points in the open ocean.

V. INITIALIZATION

A. THE PROBLEM AND SUMMARY OF THE METHOD

The purpose of the model is similar to that of atmospheric prediction models. For given initial distributions of the dependent variables (in this case temperature, surface height, and velocity) the model is to make an oceanic "forecast" of the dependent variables, subject in this case to the prescribed time-evolution of surface heating and wind stress. However, as is well known in atmospheric forecasting, the forecast problem, particularly with the unfiltered primitive equations, introduces a secondary problem of initialization which in some respects is more difficult to solve. Initial temperature distributions can be prescribed reasonably well from observation. However, except for isolated regions of strong and persistent currents, the velocity field in the general circulation of the oceans is not a directly observable quantity. It is perhaps less obvious but nonetheless true that the small spatial variations in pressure (or surface elevation) that are important in the oceanic circulation are also difficult to measure. Related to the fundamental observational difficulty is the somewhat more practical problem (from a computational point of view) of smoothing or filtering the input data. The governing equations of the present model do not filter out surface gravity waves. Arbitrarily specified initial conditions (even if known) can generate unrealistically large surface waves whose amplitudes may be comparable to the ocean depth, for instance. These constitute oceanographic noise which, to avoid contaminating the ensuing prediction, must be removed by an initialization scheme.

The problem of initialization for atmospheric prediction was apparently first investigated by Charney (1955). Many schemes have evolved since that time; for example, the global atmospheric initialization scheme of Houghton and Washington (1969). However, no comparable scheme for ocean models appears to have been published. Initialization was not considered in the published work of Crowley (1968).

The scheme worked out here is an extension of the diagnostic method of calculating currents from observed density fields as formulated by Sarkisyan and coworkers (e.g., Sarkisyan and Ivanov 1971). First, an *initial state* for surface elevation and velocity is determined for a given fixed temperature distribution. Here, use is made of two fundamental characteristics of the circulation which distinguish it from gravity-wave behavior, as pointed out by Charney (e.g., Charney 1955): its quasi-nondivergence (in the horizontal) over large horizontal distances, and its quasi-geostrophy on the rotating earth. The (geostrophic) thermal wind (or thermal current) equations appear to be sufficient to introduce a baroclinic component into the flow field without generating oceanographic noise (verified empirically).

The second part, which is analogous to the diagnostic method of Sarkisyan, consists of a time integration employing the more complete set of momentum equations. This allows for "barostropic spinup," or geostrophic adjustment of the pressure and velocity fields to the prescribed density field and boundary conditions. Temperature and wind stress are held fixed and heating is ignored throughout the initialization process.

Thirdly, the fields are (or may be) time-averaged to produce an *initialization state* which is quasi-steady for the given fixed distributions of temperature and wind stress. By this is meant that the time-averaged flow is in *dynamical* equilibrium, or nearly so. In general, there will not be thermal equilibrium, as indeed is probably the case in the real ocean. When, after initialization, heating and the temperature-prediction equation are included, the temperature will generally change. This, in turn, causes the velocity to change.

B. INITIAL STATE

The initial flow is to be nondivergent and geostrophic, i.e.,

$$\frac{\partial \zeta}{\partial t} = - \nabla \cdot H\bar{\underset{\sim}{v}} = 0$$

$$f\underset{\sim}{k} \times \bar{\underset{\sim}{v}} = - \frac{1}{\rho_\infty} \nabla \bar{p}$$

where the overbars denote vertical averages over the total depth H. It is sufficient here to take $\overline{\underset{\sim}{v}} = 0$ and $\overline{p} = \text{const}$ as initial conditions. The latter, in terms of the layer-average pressures, is

$$h_1\pi_1 + h_3\pi_3 = \text{const} \tag{5.1}$$

which, when Eqs. (3.16) and (3.17) are substituted, gives a relationship between the initial surface elevation and the initial prescribed temperature distribution. The above constant is adjusted to give zero mean surface elevation.

The condition $\overline{\underset{\sim}{v}} = 0$ gives one vector relationship between the average velocities for each of the two layers:

$$h_1\underset{\sim}{U}_1 + h_3\underset{\sim}{U}_3 = 0 \tag{5.2}$$

A second relationship comes from the thermal wind (or thermal current) equations. These are the vertically differentiated geostrophic equations in which pressure is replaced with temperature by means of the hydrostatic equation and the equation of state. In the present model the vector thermal wind equation takes the finite-difference form

$$f\underset{\sim}{k} \times (\underset{\sim}{U}_1 - \underset{\sim}{U}_3) = -\frac{1}{2} gH\alpha T_2 \tag{5.3}$$

where T_2 is the arithmetic average of θ_1 and θ_3.

Equations (5.1) through (5.3) give the initial fields of ζ, $\underset{\sim}{U}_1$, and $\underset{\sim}{U}_3$ for a specified initial temperature field. However, such fields must be modified slightly to satisfy the boundary conditions. As described in the previous section, land-coastal values of temperature are adjusted to satisfy (approximately) the insulating condition at coastlines, and coastal values of $\underset{\sim}{U}_1$ and $\underset{\sim}{U}_3$ are set to zero.

C. BAROTROPIC SPINUP AND TIME AVERAGING

The above initial state is found *a posteriori* to be sufficient to introduce a baroclinic component in the flow field without generating

unrealistic gravity-inertial oscillations. To complete the initialization we must adequately simulate the geostrophic adjustment which can take place in a barotropic (or homogeneous) fluid giving a component of velocity independent of depth (and $\bar{v} \neq 0$ in general).

A description of the spinup of a homogeneous ocean in a shallow basin of planetary scale is given by Gates (1968). We merely point out here that characteristic features of the adjustment process are the westward intensification of currents (the "Gulf Stream") accompanied by westward-propagating planetary or Rossby waves. Spinup times (measured in terms of the first peak in kinetic energy) are of the order of a few tens of days to a few months. Surface gravity waves of more moderate amplitude are in general present. Transit times for the principal gravity wave modes are of the order of $2L/(gH)^{1/2}$ ~ a few days to a few weeks, where L is a typical horizontal dimension of the basin.

The purpose here is not to study transient phenomena, but rather to generate initial fields of velocity and surface elevation which are quasi-steady with respect to given initial fields of temperature and wind stress. This is achieved in practice by employing the foregoing initial state and performing a time-integration of the primitive equation model for a period spanning about twice the spinup time, while holding the temperature and wind stress fixed. At this point the energies are inspected visually; they typically show peaks and troughs which, beyond spinup, represent oscillations between kinetic and potential energies as the sum K + P approaches a constant. For simple rectangular basins, a dominant period ~ $2L/(gH)^{1/2}$ usually shows up clearly in such oscillations, provided bottom friction is small. For more complex basin geometries there may be no single well-defined period. There may be a composite of many periods, or there may be none discernible (the latter, e.g., for a highly viscous and damped case). If peaks and troughs are discernible in the energies, the model is restarted and time-averaging performed between an integral number of chosen peaks (say) to remove the oscillations. The time-averaged fields are then substituted back and the model restarted. If the energies continue to show some appreciable oscillations, the process is repeated until a quasi-steady state is achieved for the prescribed temperature

and wind stress distributions. This represents the *initialization state*, from which predictions of temperature and velocity are subsequently made with the more complete set of equations.

The above procedure has been applied to a number of cases ranging from a simple rectangular basin to the more complex Pacific model reported on below. Typical results in terms of the energies for cases involving simpler basin geometries, and without appreciable frictional damping of oscillations, are shown schematically in Fig. 5. The geostrophic and nondivergent initial state is input at time zero. Reasonably well-defined oscillations occur between kinetic and potential energies after spinup. For a simple shallow basin with horizontal scale $L \sim 5000$ km, a time span for averaging (B - C) of 10 to 15 days is usually sufficient. Typically, only one time-averaging period was required to achieve sufficiently steady flow. The initialization state is at time C and beyond, so long as temperature and wind stress remain fixed.

Computer time requirements for this model in the complete predictive phase on an IBM 360/91 computer are less than 2×10^{-4} sec per time step per double temperature element of Fig. 2. This amounts to approximately 4 minutes of machine time per model-day for the Pacific model reported on in Sec. VI. This value compares favorably with the approximate value of 14 minutes per model-day required on the same machine by an improved, faster version of the Mintz-Arakawa global atmospheric model. Further discussion of this point is given in Sec. VII.

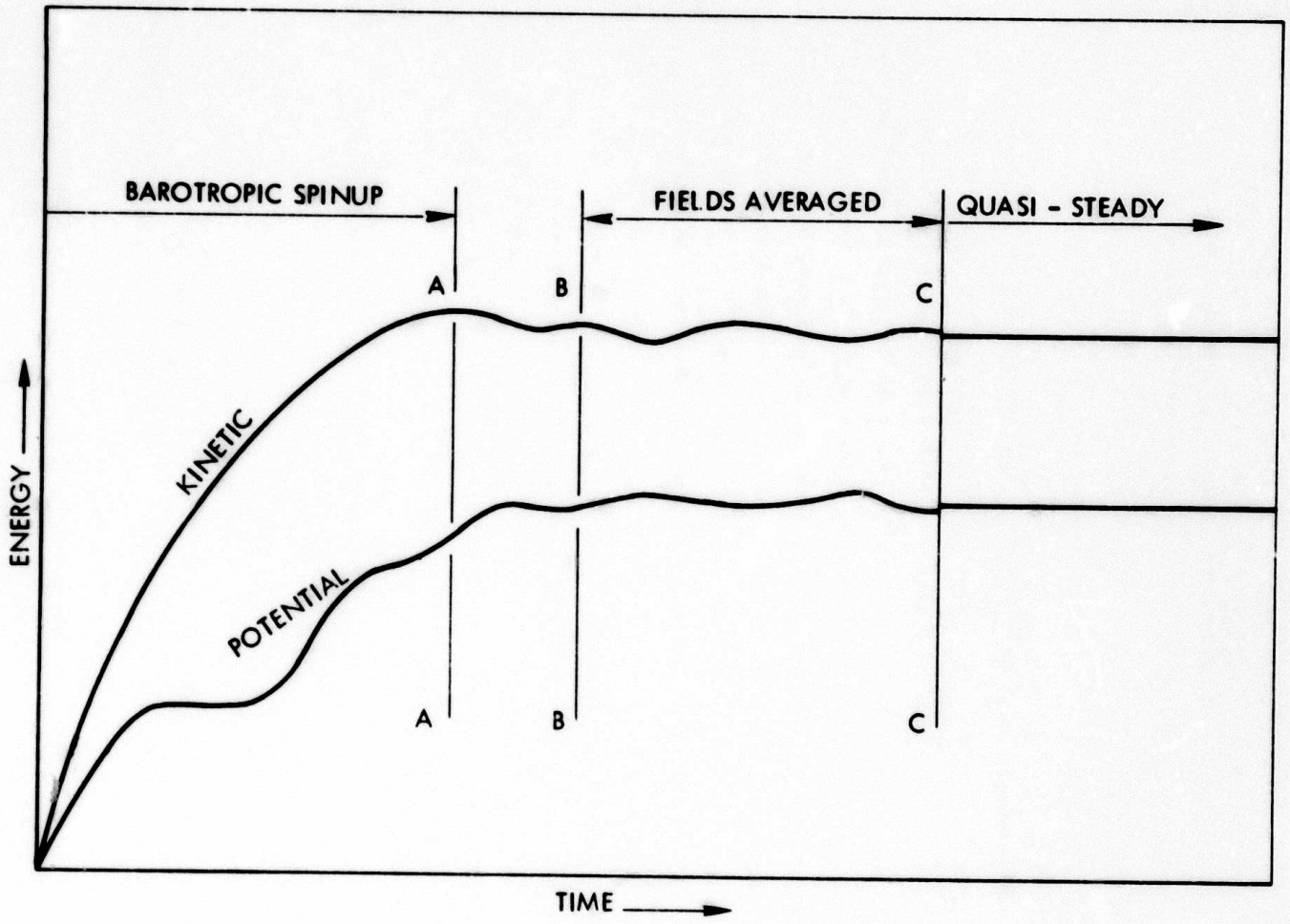

Fig. 5— Schematic behavior of total kinetic and potential energy (with respect to initial reference state) employing nondivergent thermal wind initial conditions. Temperature and wind stress are held fixed through spinup (A) and time averaging (B-C) but may be allowed to vary afterward. Averaged fields are substituted into the model which is restarted at time C. Resulting flow is quasi-steady *only* so long as temperature and wind stress remain fixed. Oscillations shown are typical of those found in runs made without bottom friction.

VI. THE PACIFIC MODEL

The basic model for an arbitrary ocean basin was described in the foregoing sections. The purpose of this section is to present results from a demonstration run for the case of the Pacific.

A. INPUT DATA

The basin extends from 80°S to 64°N. Artificial meridional barriers are placed at 105°E (just west of Australia) and across Drake's Passage at 67°W. The geography array described in Sec. IV was set up based on the data of Smith et al. (1966), who compiled global distributions of land elevation and sea depth on approximately a one-degree grid. Because the present model neglects all topographic effects, I chose (somewhat arbitrarily) the 100-m depth contour as the land-sea boundary. Grid increments are two degrees of latitude and longitude. There resulted 73 × 96 of the double elements of Fig. 2, including all artificial land elements. The array includes part of the western North Atlantic which should be ignored in the results. The array was also defined in such a way that temperature points lie on the equator. Therefore, velocity points are displaced a distance $\Delta\phi/2$ away from the equator, which avoids singularities in the geostrophic initial velocities.

Fixed parameters include the following:

Horizontal diffusion:	$A_m = 5 \times 10^8 \text{cm}^2/\text{sec}$, $A_h = 5 \times 10^7 \text{cm}^2/\text{sec}$
Vertical diffusion:	$\nu = 10 \text{ cm}^2/\text{sec}$, $\kappa = 0.3 \text{ cm}^2/\text{sec}$
Bottom friction:	$K = 2 \times 10^{-2}$ dyne-sec/cm^3 (coefficient of $\underset{\sim}{U}_3 \cong 10^{-6}$/sec)
Layer thicknesses:	$h_1 = 100$ m, $h_3 = 200$ m
Grid size:	$\Delta\lambda = \Delta\phi = 2^\circ$
Time increment:	$\Delta t = 7.5$ min

The above value of A_m is controlled somewhat by the grid size, and places the solutions in the viscous regime studied by Munk (1950). The

total depth of 300 m is of the order of magnitude required for a two-level model to resolve the strong but relatively shallow equatorial (Cromwell) undercurrent.

The above values of ν and κ were chosen also in order to model equatorial regions as accurately as possible. Arthur (1960) and Charney (1960) have recommended values of ν of order 10 cm^2/sec, while Wyrtki and Bennett (1963) and Montgomery (as reported by Wyrtki and Bennett) have recommended values of κ of a few tenths. Such relatively small values of κ are also consistent with thermocline theory for middle-latitude regions of the open ocean (e.g., Alexander 1971). (Wyrtki and Bennett recommend $\nu = 3$ cm^2/sec: however, in the present model ν is more like the vertically averaged quantity deduced by Arthur.)

The inclusion of bottom friction was motivated by a desire to reduce the number of calculations required for initialization in a demonstration run. Gates (1972a) has shown that bottom friction significantly dampens the transients generated in the spinup of a homogeneous ocean. This led me to include bottom friction under the presumptions, first, that the (reduced) energy peaks will be reached sooner, and, secondly, that time-averaging will be avoided because the transients will have almost disappeared by the end of spinup. By a simple scale analysis, the above value of K gives bottom friction forces of the same order of magnitude as horizontal friction forces.

Other input data include initial temperature fields and sea-surface distributions of wind stress and heating. These are based on January (or northern winter) conditions, motivated by comparable control and experimental runs made with a two-level atmospheric model (e.g., Gates 1972b, Warshaw and Rapp 1973). Initial temperature fields are shown in Fig. 6 based on January normal sea-surface temperature data obtained from U.S. Fleet Numerical Weather Central (FNWC) for the northern hemisphere, and National Center for Atmospheric Research (NCAR) for the southern hemisphere (as interpolated from updated global monthly normals in preparation by Alexander and Mobley 1973). Extrapolation to the lower levels of the model is based on Eq. (3.11), which relates θ_1 and θ_3 to T_1, and hence to T_0 (cf. Fig. 1). A second relation between θ_1 and θ_3 is based on thermocline theory in which I assumed

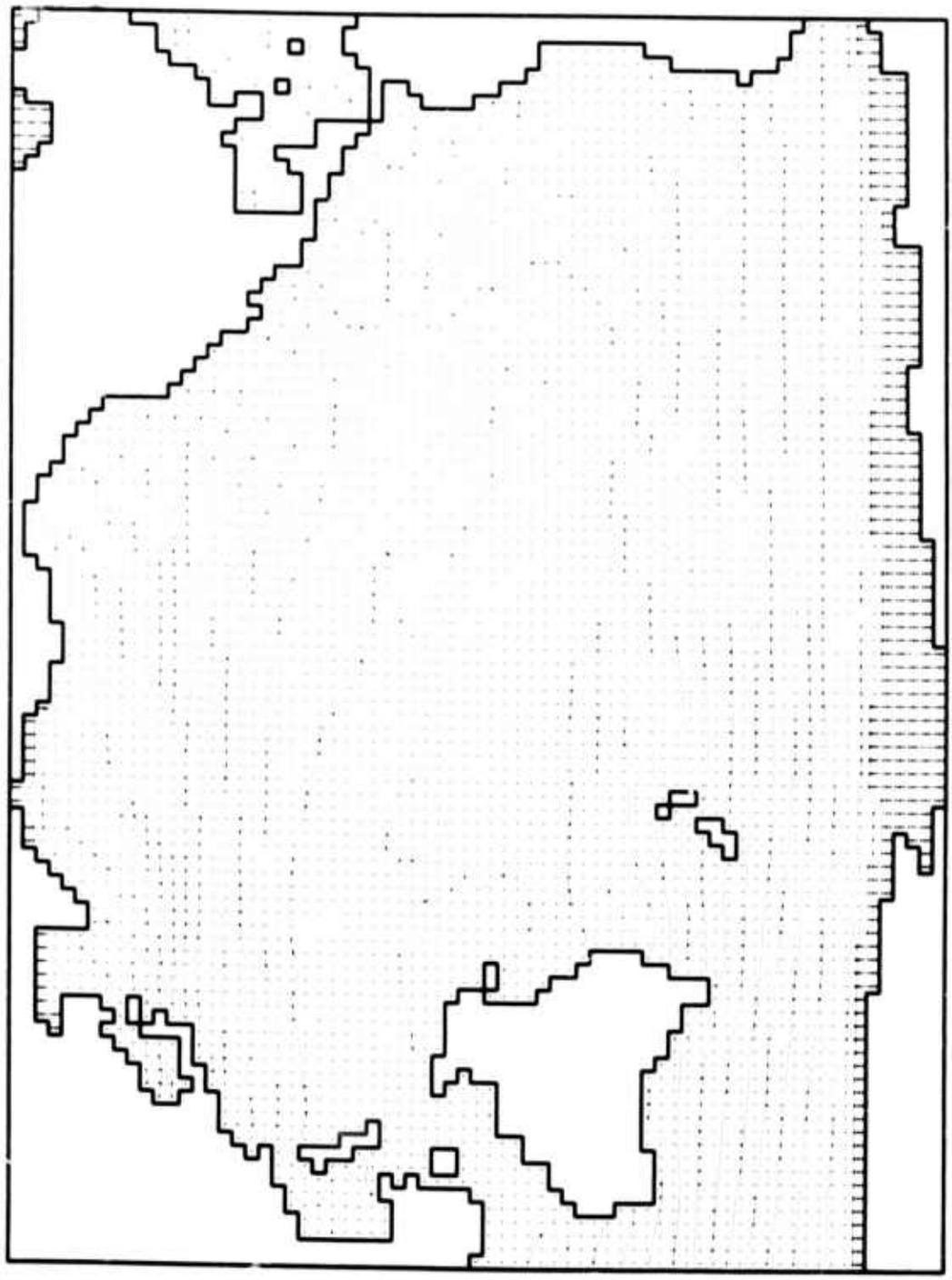

(o) Vertically averaged temperature for the upper layer, with contour intervals of 2°C and the 23-degree isotherm dashed. The closed isotherms south of Mexico/Yucatan are 25°C, and those northeast of New Guineo are 27°C.

(b) Vertically averaged temperature for the lower layer with the 15-degree isotherm dashed. The closed isotherms in northern subtropics are both 17°C. The closed isotherm west of Peru is 13°C, and that east of Australia is 19°C.

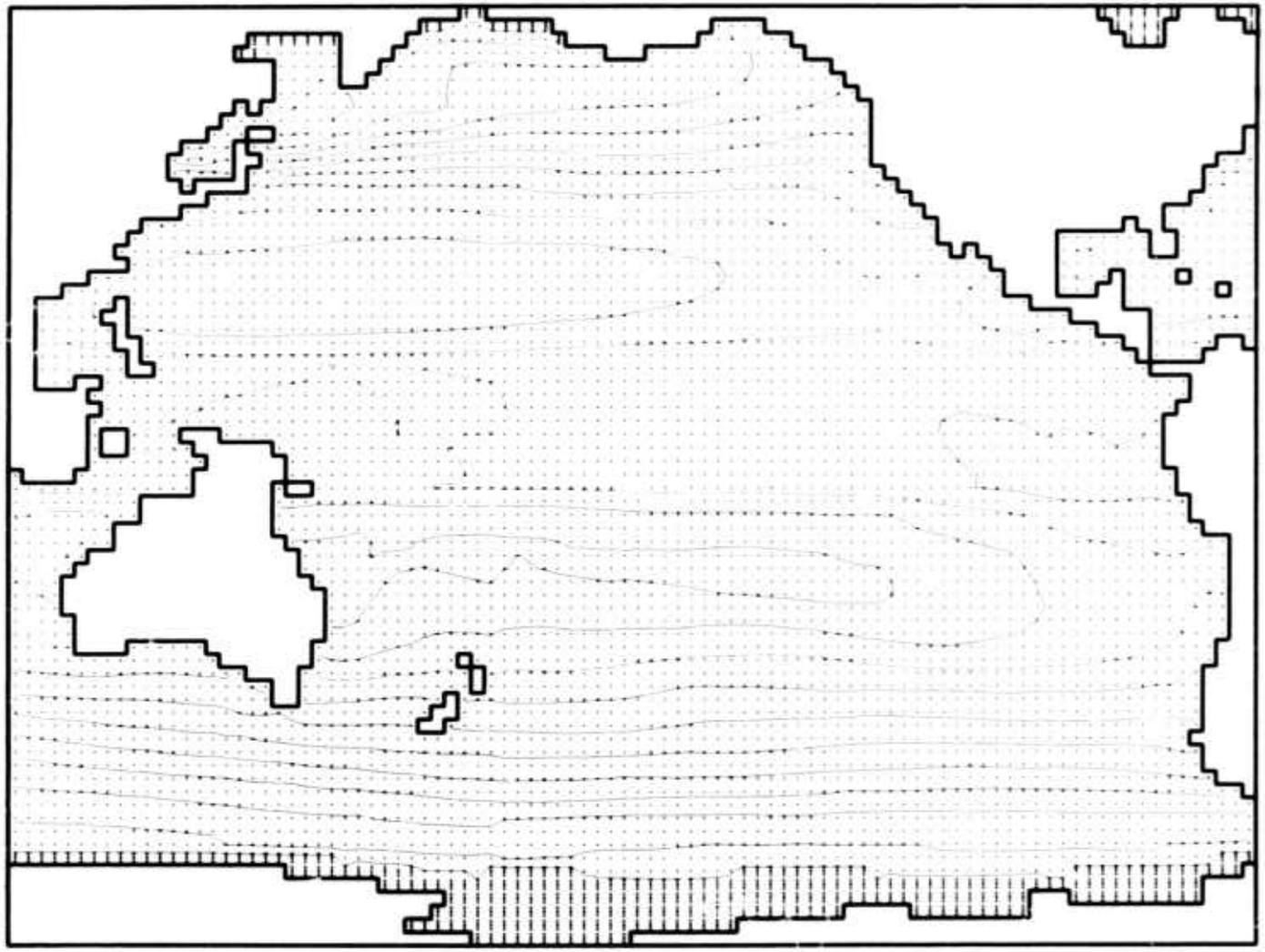

Fig. 6— Climatological January temperature fields as initial data for the model. Grid points covered by sea ice are denoted by 1. Fields were extrapolated from surface data courtesy of NCAR (Washington & Thiel, 1970) and FNWC. Land outlines based on 100 m depth contour from Smith et al. (1966).

$$\theta_3 = \theta_1 \exp(-Cz_3/D|\sin\phi|)$$

where D = 300 m is a scale-depth, and $z_3 = h_1 + \frac{1}{2} h_3 = 200$ m is the depth of the lower level. With the above scale-depth it has been shown (Alexander 1971) that a choice of the constant $C \cong 0.2$ can give results in reasonable agreement with observation. Because of the singularity at the equator, $\sin\phi$ was replaced with $\sin 10^\circ$ for latitudes between 10°N and 10°S. This is the reason for the slight discontinuity in the north-south gradient of θ_3 in Fig. 6b, noticed especially at 10°S.

Temperature distributions appear reasonable, except possibly for the eastern equatorial region in the upper layer and low latitudes in general for the lower layer. (Compare, e.g., Sverdrup et al., 1942, Charts II and IV.) At the upper level, Fig. 6a, a tongue of relatively cold water associated with the dashed isotherm ($\sim 24^\circ$C at the surface or $\sim 23^\circ$C average for the top layer) may not be sufficiently well defined along the equator toward the east. One reason for this may be the crudeness of the present grid, and the crudeness of the grids from which the normal temperature data were obtained. Also, equatorial regions are near the outer boundary of the FNWC northern-hemisphere grid.

Boundary data for the model are shown in Fig. 7. Figure 7a gives the wind stress distribution according to Hellerman (1967). Clearly evident are the familiar northeasterly (southwestward directed) trade winds in low northern latitudes. Winds along the equator are generally westward over the eastern two-thirds of the basin. A maximum wind stress of 2.6 dynes/cm^2 occurs southwest of Australia. We extrapolated Hellerman's data somewhat into high southern latitudes. However, the southernmost two rows of grid points (75°S and 77°S) contain zero values for lack of other information.

Shown in Fig. 7b is the January normal distribution of surface heating after Budyko (1963), as interpolated from the 4 × 5 deg grid data of Schutz and Gates (1971). Consistent with northern winter conditions, the North Pacific is generally being cooled, and the South Pacific (except high southern latitudes) generally heated. Maximum cooling of about 780 ly/day occurs just east of Japan. Again, because

data were not available in high southern latitudes, the heating there was arbitrarily set to zero. This may not be important in the model because much of the region is covered by the main ice pack. Here, as described in Sec. IV, the temperature is held fixed at $-1.9^{\circ}C$ and the heat equation ignored. (Compare the ice-covered region in Fig. 6.)

B. RESULTS

The initial state for surface elevation and the velocities was determined employing the procedure of Sec. V for the given fixed temperature distributions of Fig. 6. The resulting surface elevation is shown in Fig. 8a. Note the rough similarity between this pattern of isolines and the pattern of isotherms shown in Fig. 6a. This results from the initial condition (5.1) relating surface height to the temperature distribution. The initial velocities, not shown, give equal and opposite transports in each layer from the initial condition (5.2).

Spinup proceeded subject to the wind stress of Fig. 7a, with temperature held fixed and surface heating and the heat equation ignored. As expected, bottom friction was apparently sufficient to damp the oscillations generated during spinup. Kinetic energy reached a peak near the end of day 79 and then began to decline slightly. The behavior of the energies near spinup is shown on an expanded scale in Fig. 9. The change in total energy, kinetic plus potential, is less than 0.1% between day 74 and day 90. Inspection of the fields at 5-day intervals confirmed that the flow was sufficiently steady after about day 74 to represent an initialization state for the prescribed temperature distribution. (Such inspection, taken by itself, is hardly proof of steadiness because 5-day periodicity, for example, would not show up. However, no 5-day or shorter-period oscillations are apparent in Fig. 9.)

Surface elevation at the end of 90 days is shown in Fig. 8b. Well-defined subtropical high-pressure cells appear in northern and southern middle-latitudes, and the northern subpolar low-pressure cell is probably realistic. Not much significance should be attached to the southern, very deep, low-pressure cell because of the artificial meridional barriers. One encouraging factor is the more diffuse nature of the

(a) December-February normal distribution of surface wind stress interpolated from Hellerman (1967). The half-arrows give the direction of stress, and the isolines give magnitudes in units of 0.3 dynes/cm^2. The dashed line is 0.9 dynes/cm^2.

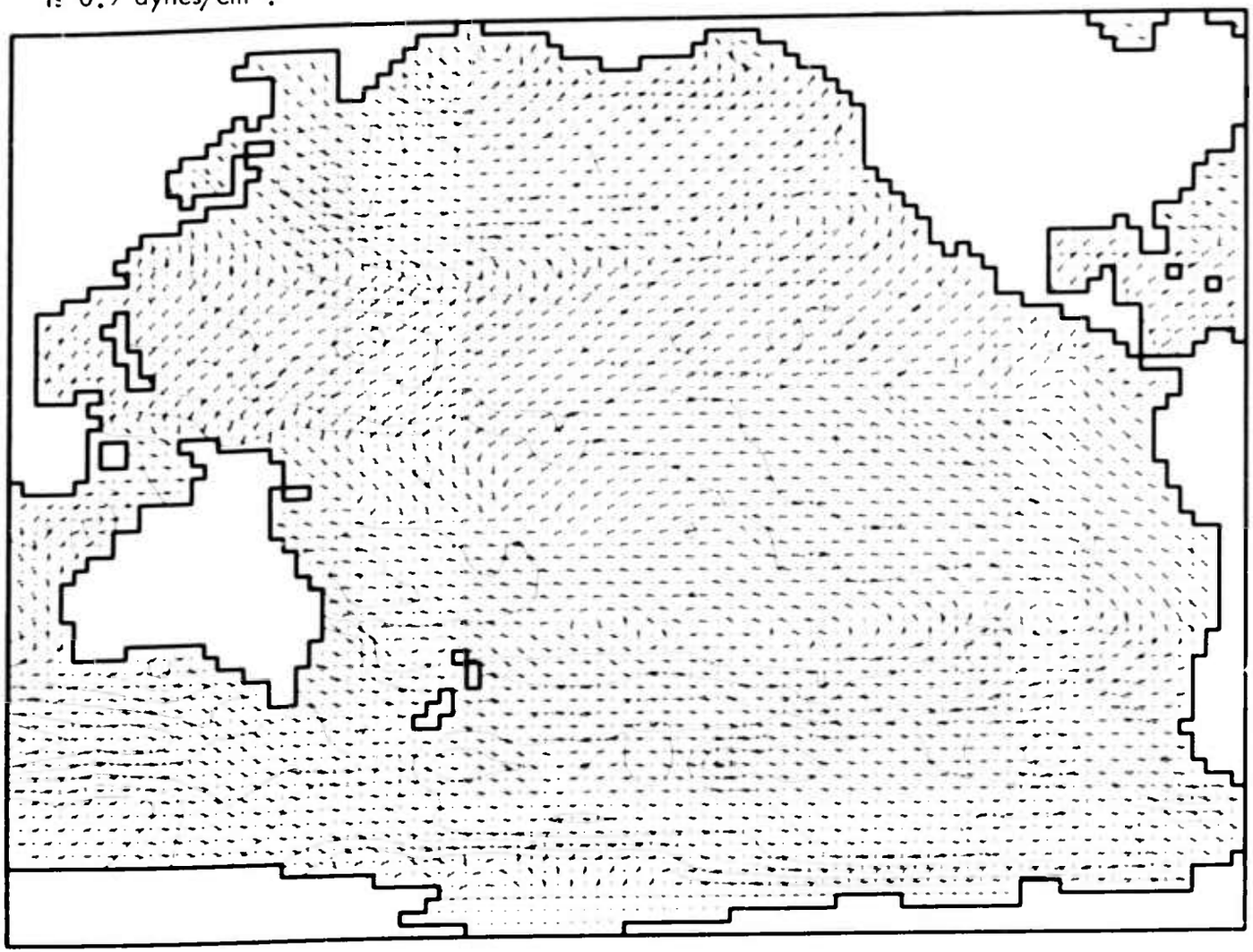

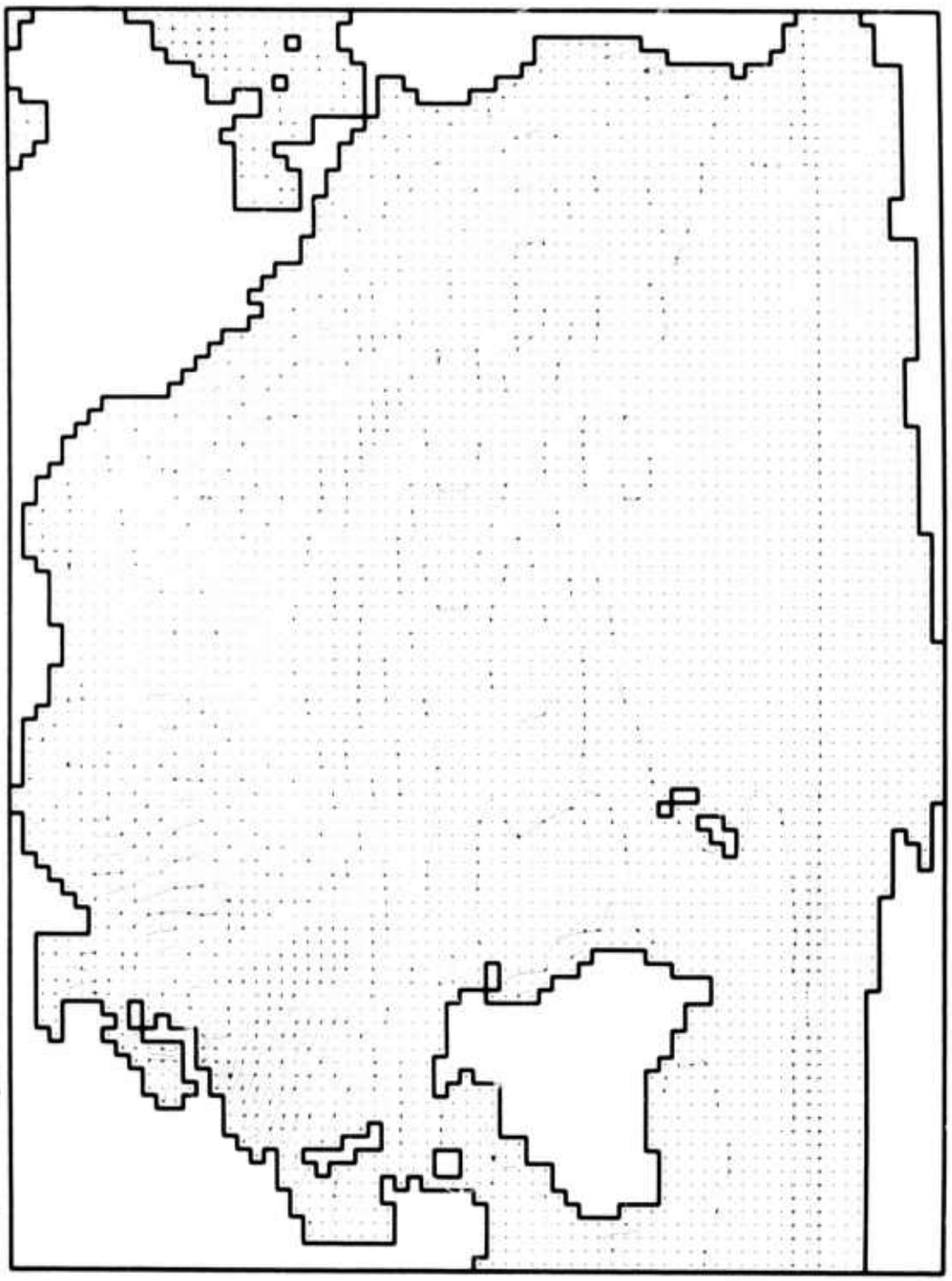

(b) January normal surface heating according to Budyko (1963), as analyzed by Schutz and Gates (1971). Contour intervals are 50 ly/day, and the dashed line denotes zero. A maximum cooling of 775 ly/day occurs just east of Japan.

Fig. 7 — Boundary data for the model.

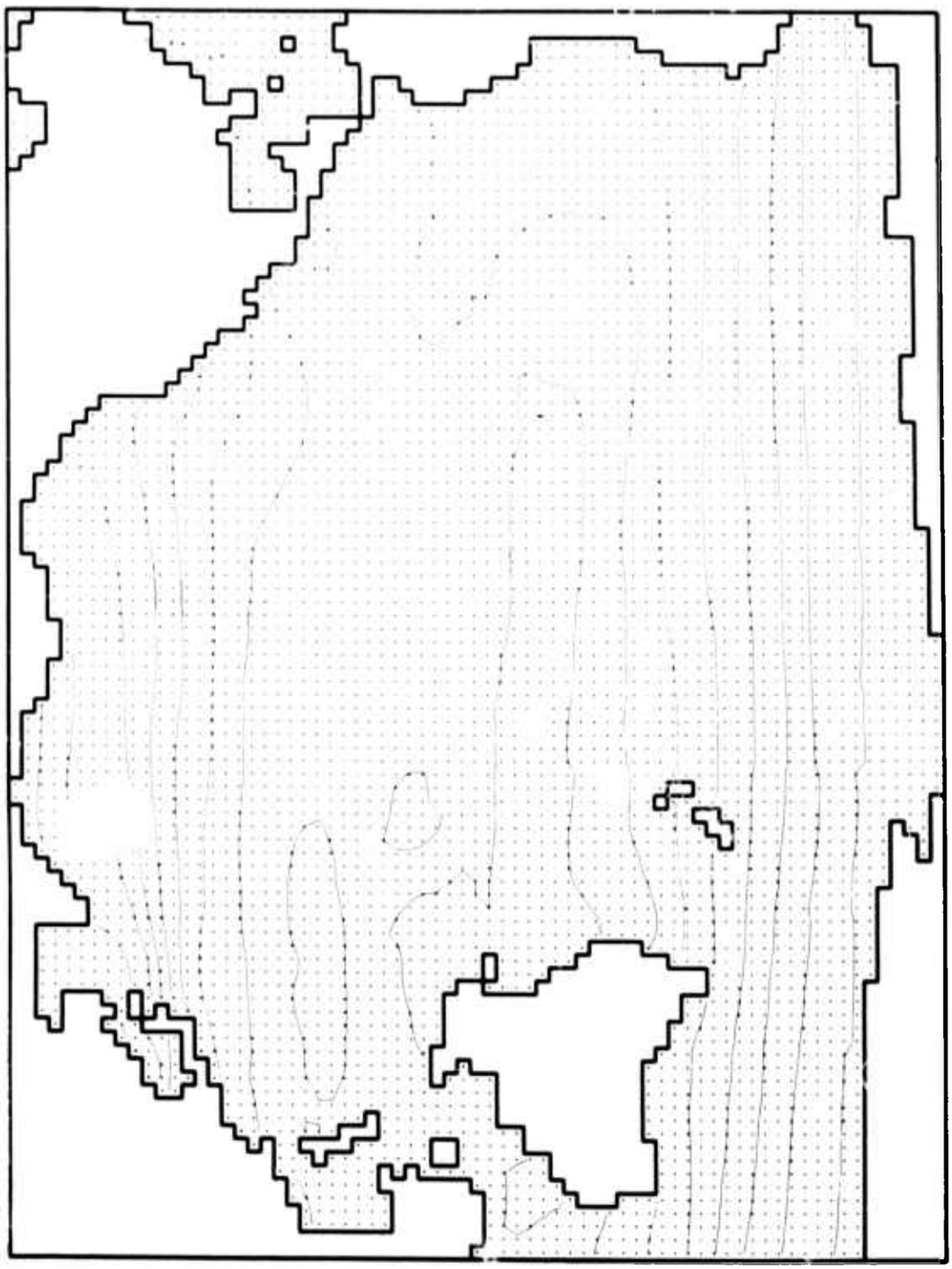

(a) Initial surface elevation based on non-divergent and geostrophic initial conditions applied to the temperature fields of Fig. 6. Elevations are positive in low latitudes, negative in high latitudes.

(b) Surface elevation at the end of 90 days (initialization state) with temperature held fixed. Note the smaller gradients east of Australia compared to those in the Kuroshio Current.

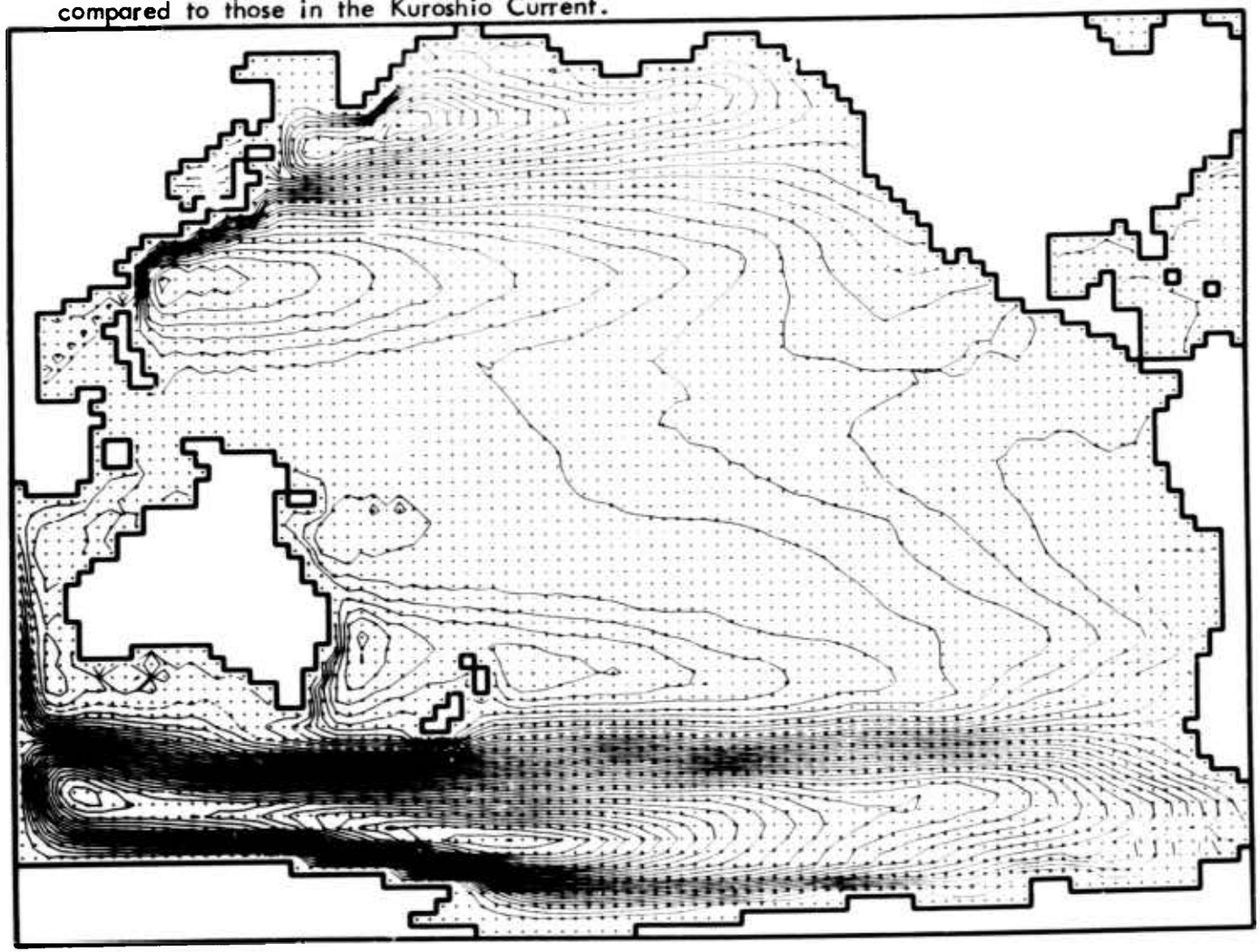

Fig. 8 — Initial and predicted surface elevation with respect to mean sea level. Contour intervals are 10 cm, and the dashed line denotes zero elevation.

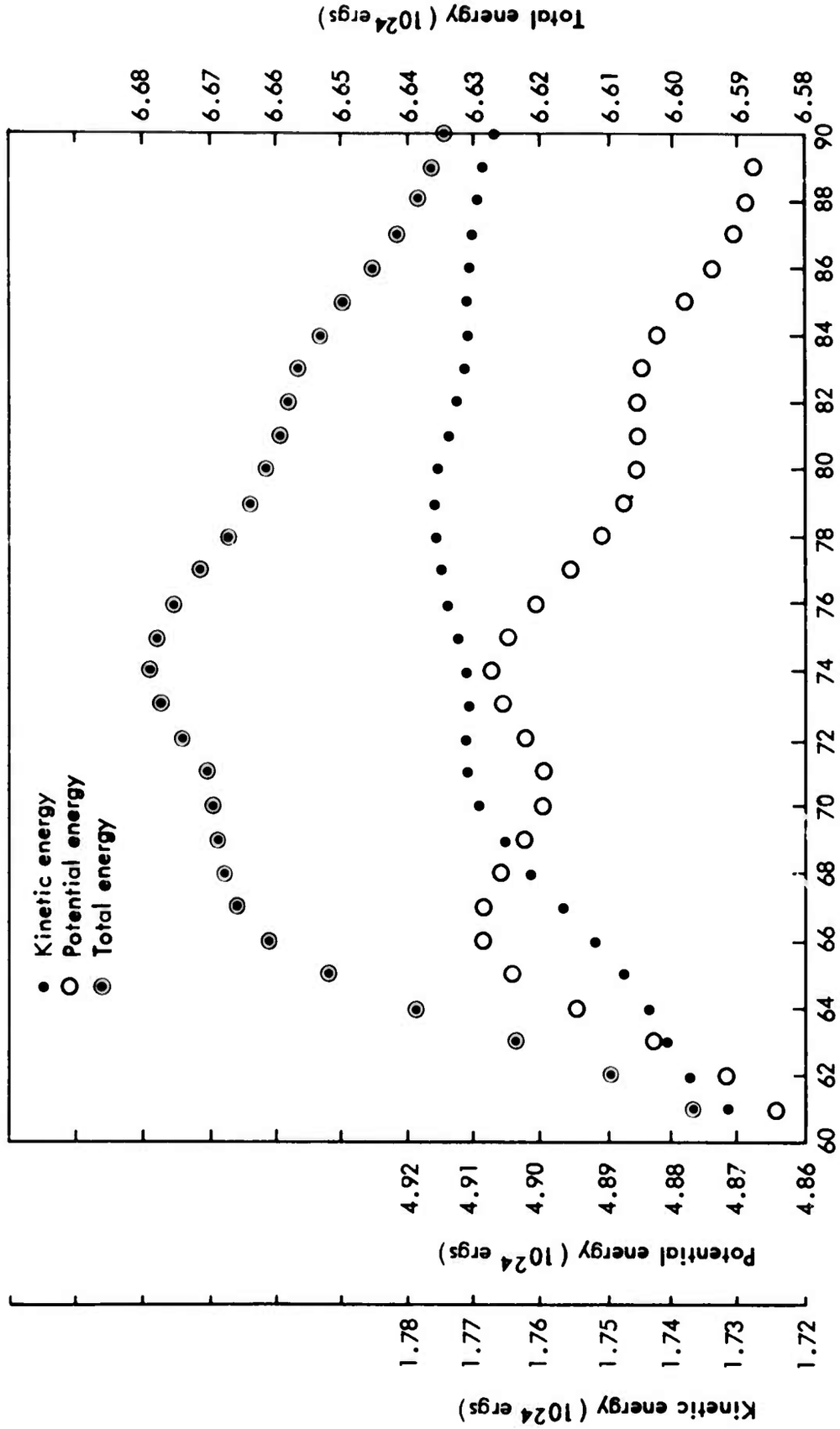

Fig. 9— Detailed behavior of energies near spinup. Note the expanded scales. Potential energy at day 90 is 0.8% less than its value at day 74. Temperature and wind stress are held fixed throughout initialization. The more appreciable oscillations depicted schematically in Fig. 5 do not occur in this run because of bottom-friction damping.

high-pressure cell east of Australia compared with its counterpart to the north, indicating that the East Australia Current will be weaker than the Kuroshio, in rough agreement with nature. However, the strong gradient at the meridional barrier west of Australia indicates a totally unrealistic current there, as expected. Along the equator the surface elevation increases toward the west, consistent with the piling-up of water under a westward-directed wind stress.

The small-scale diamond patterns and sawtooth patterns in Fig. 8b, e.g., west and east of the Philippines, respectively, are computational and not physical. They represent slight solution separation that is inherent in the central space-difference scheme used, apparently generated by the computational boundary conditions. Such separation appears by the end of day 20 in the present integration, but does not worsen significantly throughout the subsequent calculations.

The resulting initialization state for the velocities is shown in Fig. 10. Probably the most realistic region is the North Pacific. The relatively strong Kuroshio current appears near the Philippines and Japan. Its maximum values are nearly 60 cm/sec at both levels; these are somewhat on the low side compared with observed values of 1 to 2 m/sec, but are consistent with the crudeness of a two-degree grid resolution. The Kuroshio extension, roughly the region extending eastward to the 10 cm/sec isoline, is reasonably well defined, as is its further extension into the North Pacific Current, generally the region bounded by the dashed (5 cm/sec) isoline. The Alaska current and the southward-flowing Oyashio to the west appear reasonable. (Compare, e.g., Sverdrup et al., 1942, Chart VII.) The southward drift in eastern middle latitudes might be termed the California Current although it does not extend southward of California in the model. This may be consistent with nature in the northern winter (e.g., the discussion in Sverdrup et al., 1942, p. 725, of the northward-flowing Davidson Current). The westward-directed North Equatorial Current is well defined in latitudes of about 15°-20°N in the model.

The flow in low latitudes is unrealistic in several ways (partly corrected in the ensuing prediction). Principally, the flow may not be sufficiently east-west, but has significant poleward components in the

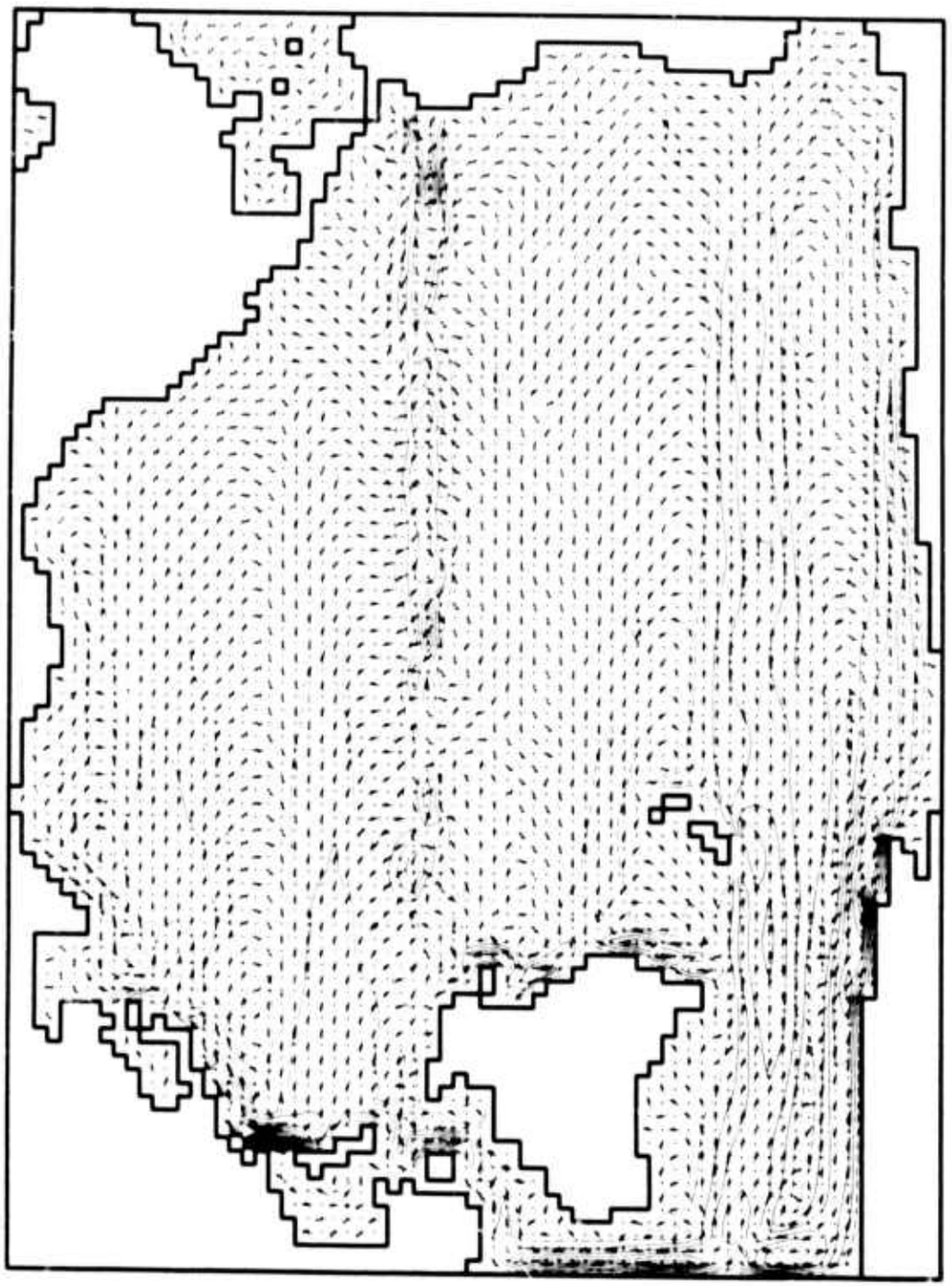

(a) Vertically-averaged velocity for the upper layer.

(b) Vertically averaged velocity for the lower layer. Maximum speed occurs in the Kuroshio and is nearly 60 cm/sec at both levels.

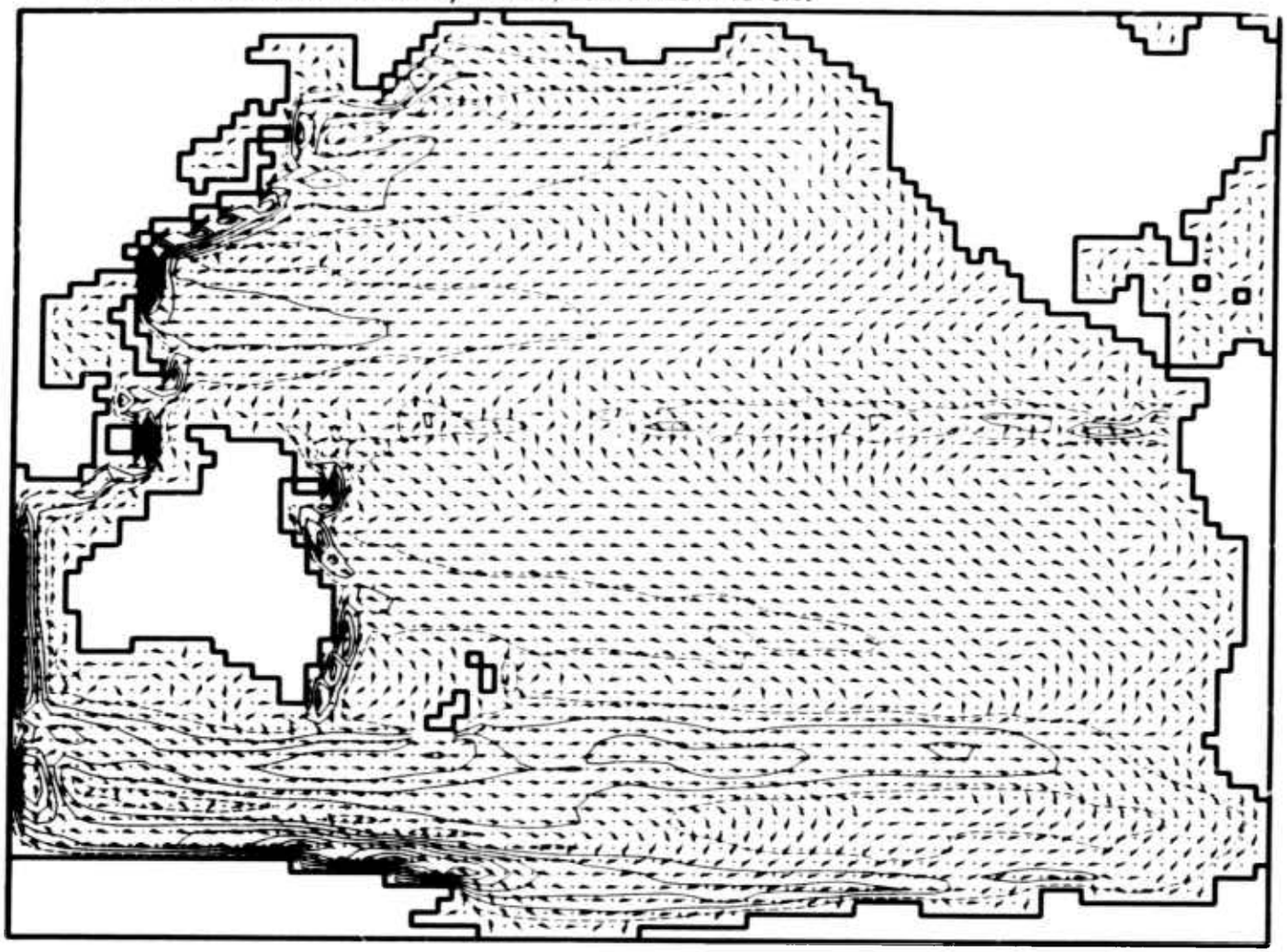

Fig. 10 — Initialization state for the velocity fields. The direction of flow is given by the half-arrows, with speed contoured in increments of 5 cm/sec; the 5 cm/sec isoline is dashed.

upper layer, equatorward in the lower layer, as can be seen in Figs. 10a and b, respectively. Slightly realistic aspects are the larger speeds depicted by the isolines near the equator, and the tendencies for equatorial velocities to have some westward component in the upper layer, and some eastward component in the lower layer. As demonstrated presently and discussed in Sec. VII, the unrealistic meridional components near the equator are caused by an inaccurate specification of initial temperatures in low latitudes.

The flow in eastern low latitudes is generally confusing. In low southern latitudes a northward-flowing "Peru Current" has left the coast at central Chile. If anything, there is southward flow (in the upper layer) off Peru, suggesting severe *El Nino* conditions to an extent probably never observed (cf. Sverdrup et al., 1942, p. 704).

Encouraging features in the South Pacific include the weaker and more diffuse nature of the East Australia Current compared with the Kuroshio. However, the strong currents at the meridional barrier west of Australia are unrealistic as expected, as is the flow in high southern latitudes.

A fifteen-day prediction is now made in the sense that temperature is allowed to change subject to the heat equation, and subject to the surface heating of Fig. 7b and the (approximately) insulating boundary conditions. However, the temperature at ice-covered points continues to be fixed at $-1.9^{\circ}C$ as described in Sec. IV. The wind stress of Fig. 7a is also held fixed for this experiment. The resulting changes that occur in velocity and temperature are most pronounced in equatorial and eastern tropical regions.

The temperature distributions at the end of day 105 are shown in Fig. 11. The most striking feature is the tongue of relatively cold 23-deg water that has developed in the upper layer in the eastern equatorial region (Fig. 11a). The tongue, which is centered almost exactly on the equator, appears to be in rough agreement with Chart II (February distribution) of Sverdrup et al. (1942). (In Fig. 11a, $23^{\circ}C$ corresponds roughly to 24-deg surface water.) Temperature reductions in excess of $1^{\circ}C$ have occurred in the eastern equatorial region. The region of 27-deg water to the west has been reduced slightly in size

compared with the initialization state, and the maximum temperature is now 27.9°C, compared with 28.2°C before the prediction. This feature may be somewhat less in agreement with observation.

In the lower layer (Fig. 11b) the situation is similar in that most of the changes occur in low latitudes. The tongue of 13-deg water toward the east has increased in size and has become more nearly centered on the equator. Toward the west the region of water with temperatures in excess of 15°C has become larger. (The region bounded by the dashed line with temperatures less than 15°C is now smaller.) However, a cooling trend has occurred in the immediate vicinity of the equator as evidenced by the westward extension of the 15-deg water.

Generally, at both levels the equatorial region has been cooled, and at the same time, the east-west temperature difference has increased. Elsewhere, very little has changed. Small-scale irregularities have been smoothed slightly from the effect of horizontal eddy diffusion in the model. Slight changes from advection as well as diffusion can be seen in the Kuroshio and East Australia Current regions. The temperature pattern southwest of Australia has changed as a result of the unrealistic current there.

The velocity fields at the end of day 105 are shown in Fig. 12. Again, most of the changes have occurred in low latitudes, and perhaps the most striking feature is the zonal flow that has developed near the equator. In rough agreement with nature, the flow is directed westward in the upper layer, eastward in the lower (~ Cromwell Current) layer. However, the speed in the lower layer, ~ 10 cm/sec, is small by a considerable margin compared with Cromwell Current speeds of order 100 cm/sec. The discrepancy arises at least partly because the velocities are layer-average values (cf. Fig. 1). Thus 10 cm/sec applies to the entire lower layer of thickness 200 m.

The flow in the California and Peru Current regions remains confusing. In addition, there are no North- and South-Equatorial countercurrents (eastward-directed) in the upper layer. This may be partly related to a relatively large horizontal grid spacing.

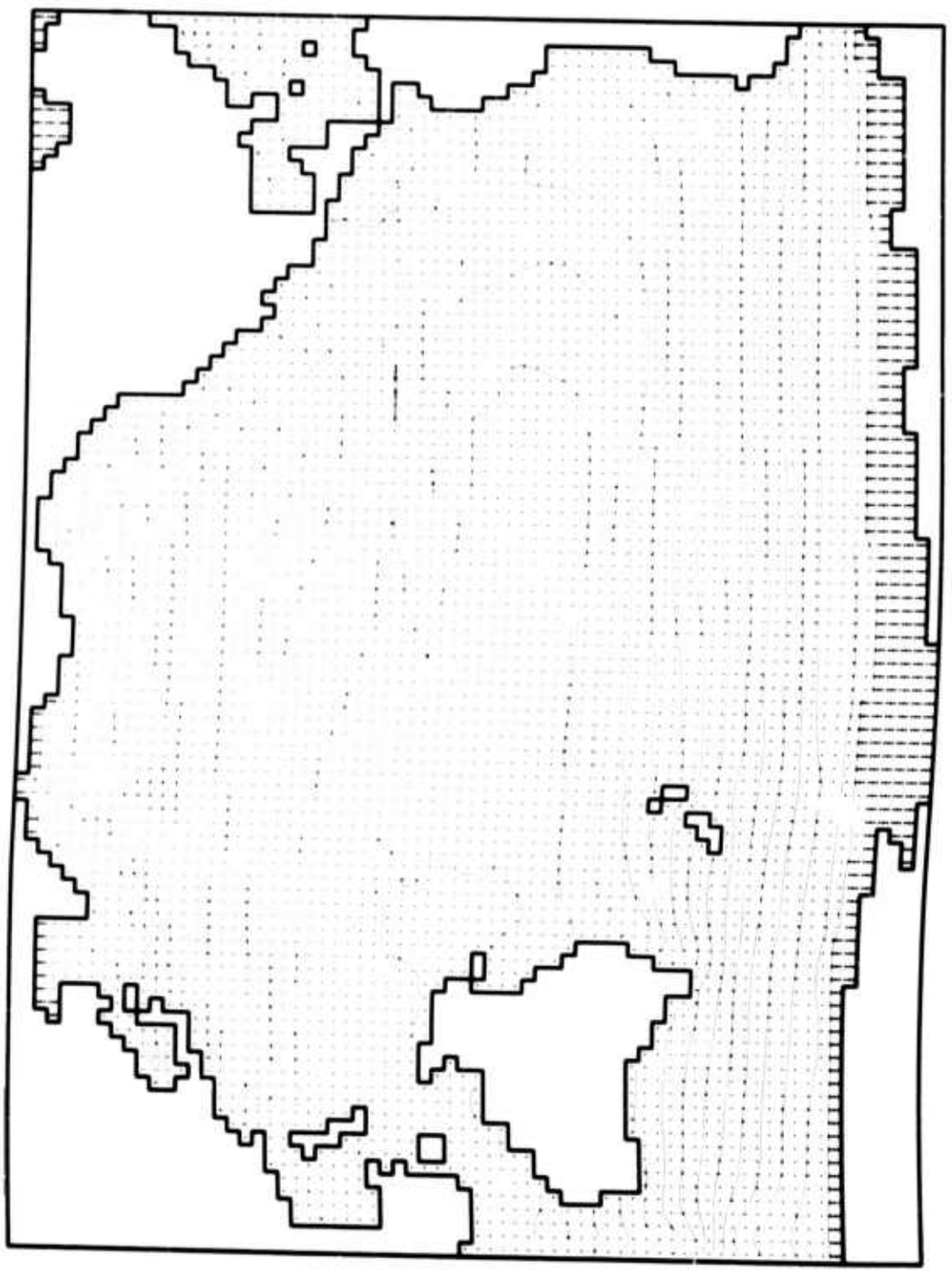

(a) Vertically averaged temperature for the upper layer. Note the tongue of 23-degree water along the equator toward the east.

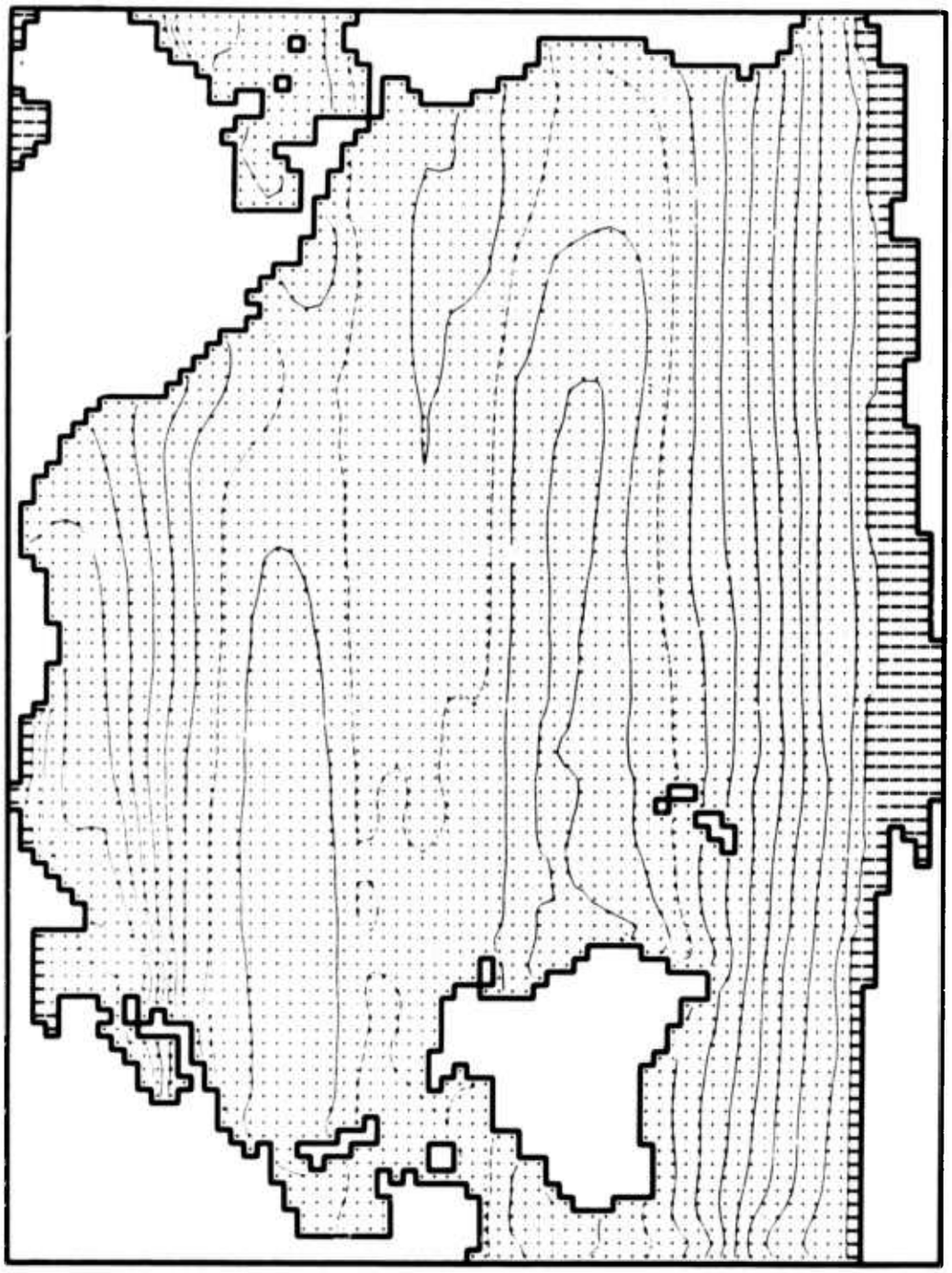

(b) Vertically averaged temperature for the lower layer.

Fig. 11 — Fifteen-day prediction of temperature fields (end of day 105) subject to the heating of Fig. 7b. Contour intervals and dashed lines same as Fig. 6.

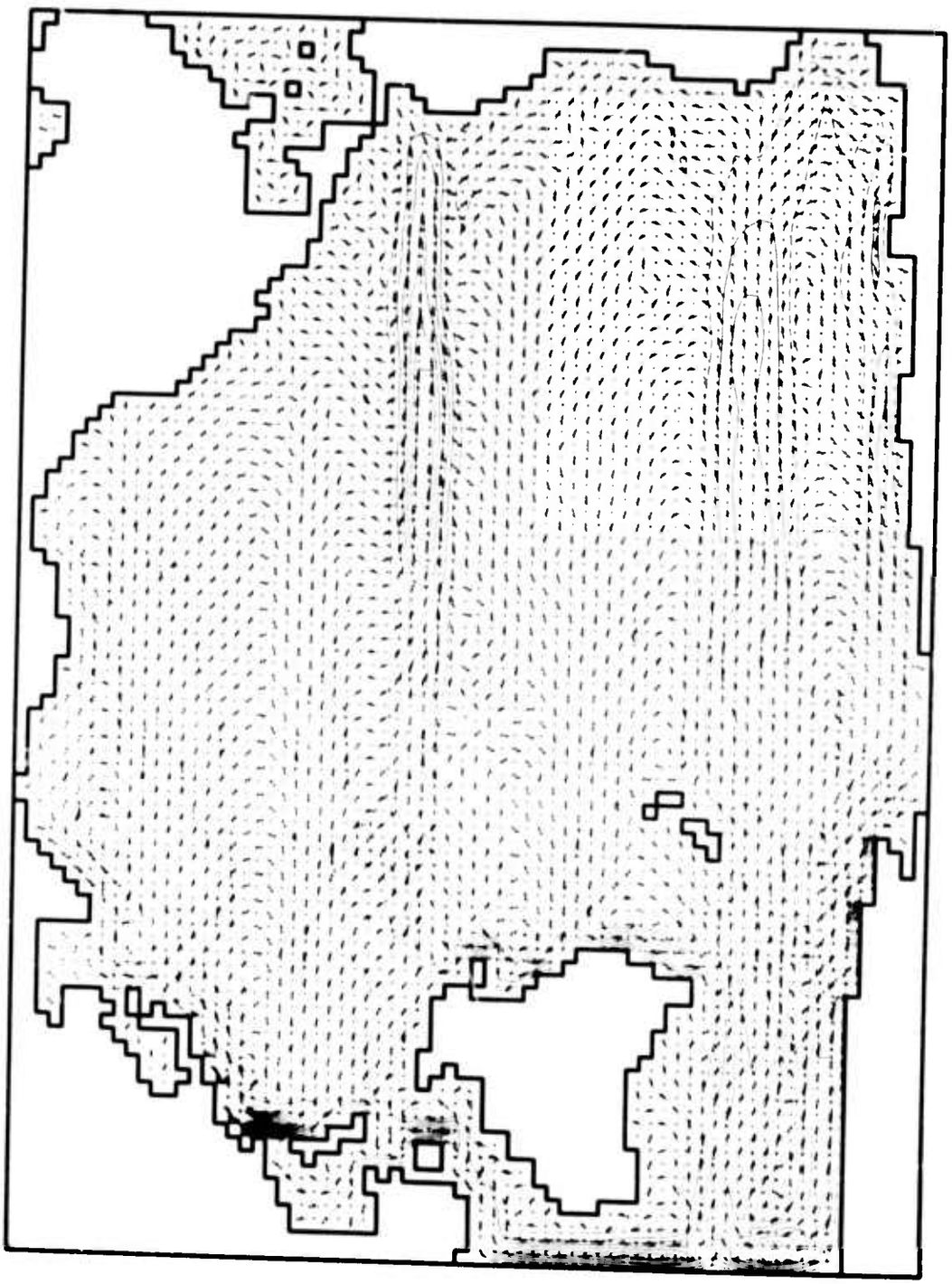

(a) Vertically averaged velocity for the upper layer.

(b) Vertically averaged velocity for the lower layer. Note the more realistic east-west velocities near the equator at both levels.

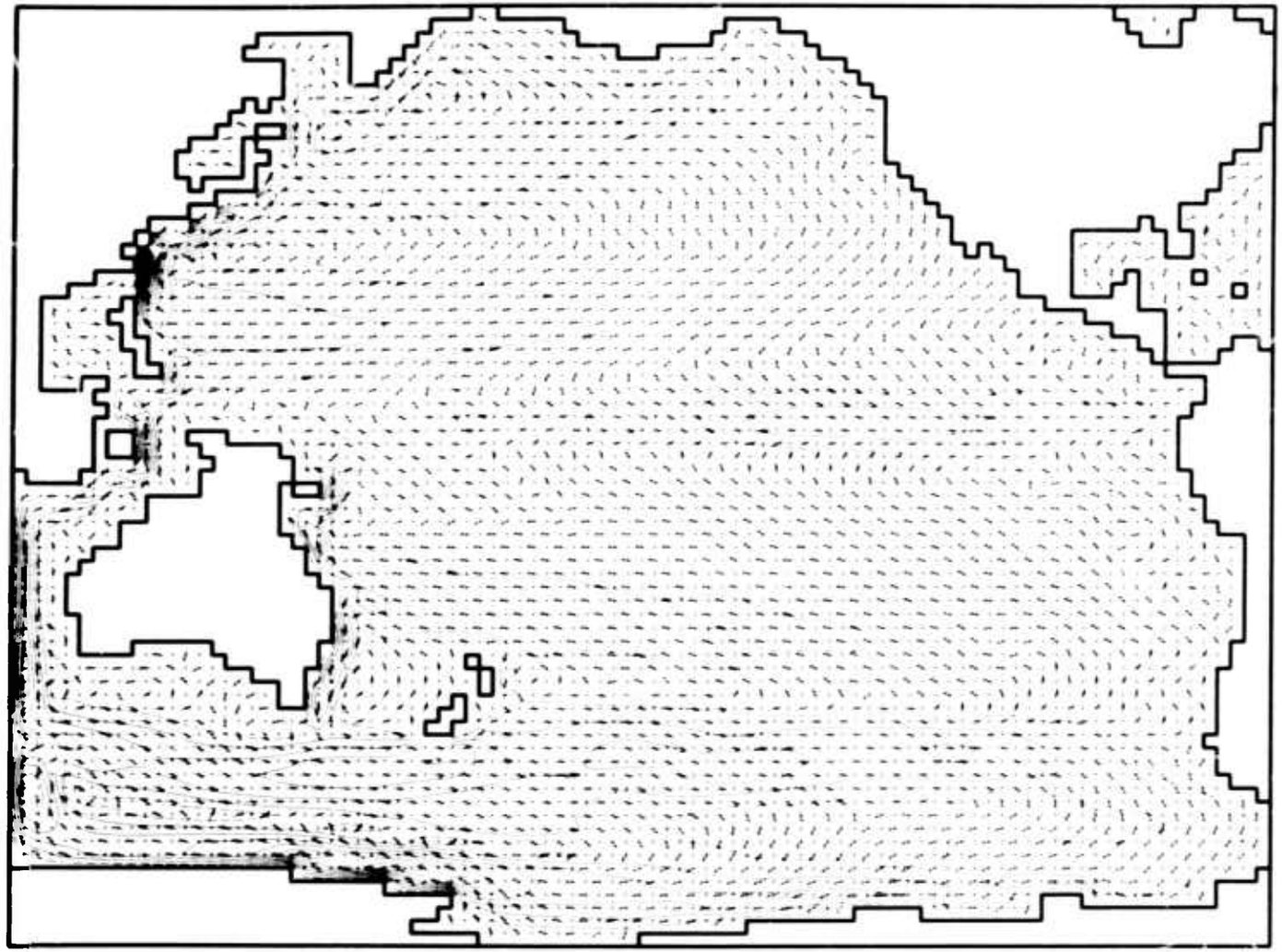

Fig. 12 — Predicted velocity fields at the end of day 105. Arrows and isolines have same meaning as in Fig. 10.

VII. DISCUSSION AND CONCLUSIONS

The results from the Pacific model are generally encouraging. Perhaps to some extent they are also surprising, in that an ocean model can apparently make 15-day predictions showing appreciable changes (of order $1^{o}C$) in the temperature distributions, at least in equatorial regions. The thermal inertia of the ocean is large compared with that of the atmosphere. But this apparently does not preclude appreciable oceanic changes (in the model) on time scales of order 10 days for the upper layers in low latitudes. This may have important implications for monthly and seasonal simulations with interacting atmospheric and oceanic models.

There are, of course, a number of deficiencies in the Pacific model. For the most part these might have been anticipated from the known limitations of the model design. The model should not be taken too seriously near eastern boundaries, where it generally predicts *downwelling*. This seems to be a characteristic shortcoming of general circulation models with coarse grid spacing (e.g., Bryan and Cox 1967). It is likely that inclusion of continental slope and shelf topography, as well as much finer horizontal grid resolution, will be required before models such as this can adequately simulate upwelling near the western shores of continents.

Regarding the confusing flow in the eastern tropical region, it is less clear what the cause might be. It is doubtful that the southward-flowing (*El Nino*) current can be believed to extend to northern Chile, because such an event has apparently never been observed. The fault may lie either with the model, or with the input data (wind stress, heating, and initial temperatures), or both. For example, neither the coarse grid-resolution of the model nor that of the input data can adequately resolve the smaller-scale temperature structure observed near Peru. (See, e.g., Wyrtki 1969.) This problem is at least partly related to the upwelling difficulty.

A related limitation is that the model does not predict mixed-layer thickness, but rather assumes it to be uniformly 50 m (one-half the

upper-layer thickness of Fig. 1). The limitation is not quite that severe because the model can predict, e.g., $\theta_1 = \theta_3$ at some point, in which case the mixed layer extends locally to 300 m depth. Nevertheless, this is one of several limitations motivated largely by a desire for simplicity. A variable mixed-layer thickness would add still another prediction equation to the model. The strategy has been to try to extend the simpler model as far as possible, recognizing that improvements might, and probably should, be added later.

As a consequence of the assumed constant levels of Fig. 1, the choices made for layer thicknesses represented trade-offs among many conflicting requirements. For example, a horizontal bottom associated with the base of the main thermocline in middle latitudes might be placed more realistically at 600 m to 800 m depth. However, it seemed more important to attempt a better model for the vast tropical region. Here, the relatively shallow Cromwell Current dictated a bottom depth of perhaps 300 m for a two-level model. The latter was the decisive factor in this instance. However, the assumption of zero vertical velocity-shear in the lower half of the lower layer (cf. Fig. 1) is perhaps more of a compromise in favor of middle latitudes. In the Cromwell Current, appreciable vertical shears extending to 300 m depth and beyond have been reported by Knauss (1960) and others.

In spite of these and similar criticisms of the model, the results on balance are encouraging. The ocean model with its coarse grid may be unable to resolve the small-scale temperature structure off Peru; but neither could a (hypothetically) coupled atmospheric general circulation model with its even larger grid spacing. Perhaps the most encouraging factor arises from an apparent paradox in the results: we input observed data, initialized the model, and then made a "forecast." If the data and the model were both "correct," then the forecast might have properly been for *no change*. However, the real ocean is probably never in equilibrium. Moreover, there is no obvious reason to expect consistency among an ocean model on the one hand, and distributions of temperature, wind stress, and heating on the other, all produced by different investigators working independently of each other. Our input temperature data were apparently incomplete and inconsistent with the

model in the equatorial region. The encouraging factor is that the model predicted the cold tongue of water toward the east, a prediction that seems to be in better agreement with observation, and which is of sufficient extent that it might be detectable by an atmospheric circulation model.

None of the foregoing is meant to suggest that the *prediction* of a cold geographic equator and zonal flow is anything new. Haney (1971a) found a similar result with a filtered, six-level model of a rectangular ocean. One point of distinction concerns *time scales*, which are vastly different: 200 to 210 years in Haney's case (the model times for which Haney presents results) versus 90 to 105 days in the present, unfiltered model. The purposes of the two models are also different. Haney's, much like the early models of Bryan and Cox, has the major purpose of studying the long-term, steady-state response of the oceans. His model is more satisfying in the sense that it is able to predict features starting from simpler initial conditions, e.g., isothermal and a state of rest. The present model cannot do this because its time increments are much too small. Rather, its stated purpose is to make short-term, monthly and seasonal predictions, and the present model must be initialized from observed data. Thus, in another sense the present model may be more satisfying as a shorter-term prediction model. The point is that the predicted rapid response of order 10 days in low latitudes appears to be new.

The predicted zonal flow and temperature anomaly at the equator (anomalous from an atmospheric point of view) might be further criticized as being too special. Although the stated purpose of this work is to develop a world ocean model for climate experiments, and not to investigate equatorial effects as such, there are, nevertheless, valid questions. How sensitive is the result to the initial temperature distribution? or to the applied wind stress? or to the basin geometry?

The foregoing result was in fact found to be typical of several runs made with the Pacific model, and of many runs made with earlier, simplier versions. The simplest case was that of a (two-level) homogeneous ocean in a rectangular basin subject to a simple zonal wind stress distribution having a westward component at the equator. Comparison runs for different vertical viscosities and layer thicknesses

all showed the same qualitative results near the equator. The zonal *components* of flow, westward (eastward) at the upper (lower) level, were often realistic. However, the meridional components were generally at least as large, and these were poleward (equatorward) at the same respective levels. (Pure zonal flow can of course occur *at* the equator for north/south symmetry of the boundary conditions.)

Qualitatively similar results were obtained in the simple baroclinic comparison runs--but only for the initialization state--whenever the initial temperature was a specified function of latitude and depth, but not of longitude. Predictions then showed the simultaneous development of more realistic zonal flow near the equator together with an east-west temperature gradient, with colder water toward the east. However, well-defined countercurrents displaced north or south of the equator were generally not found in the results. This difficulty was also encountered by Haney (1971a) with a six-level model. The point here is that the foregoing results in the equatorial zone were not an isolated, special case. The results suggest that the observed zonal flow near the equator and the temperature anomaly toward the east may be intimately coupled. However, a physical explanation is not offered here, and further study with a more specialized equatorial model is required to clarify this point.

A final encouraging factor from the Pacific model is the speed of the calculations. As mentioned at the end of Sec. V, approximately 4 min of IBM 360/91 machine time are required per simulated day of the Pacific model on a 2 × 2 deg mesh. Doubling this gives approximately 8 min/day for the global case, a conservative estimate providing high-latitude boundaries are maintained for linear computational stability. Increasing the 2 × 2 deg mesh size to the 4 × 5 deg global mesh in current use with the Mintz-Arakawa model gives a coarse-grid case for direct comparison. Computer times in the coarse-grid case, taking into account the allowable increase in time increment, should decrease by a factor of ten or so. This gives less than 1 min/day compared with about 14 min/day for the faster version of the Mintz-Arakawa model. Thus, computer times for the global ocean model may be only a tiny fraction of the total time required in projected atmosphere-ocean model

experiments, but in any event no more than perhaps one-third, depending on the mesh size.

In conclusion, the Pacific model is able to simulate reasonably well most of the gross features of the circulation and temperature distribution in the upper ocean. The model is able to predict temperature changes of order $1^{\circ}C$ on time scales of order 10 days in low latitudes, indicating that projected monthly and seasonal simulations with a coupled atmosphere-ocean model may be productive. Finally, computer costs appear modest for an unfiltered model. The Pacific model is now being extended to the world ocean case, with possible improvements postponed to later.

REFERENCES

Alexander, R. C., 1971, "On the Advective and Diffusive Heat Balance in the Interior of a Subtropical Ocean," *Tellus*, 23, 393-403.

Alexander, R. C., and R. L. Mobley, 1973, *Updated Global Monthly Mean Ocean Surface Temperatures*, The Rand Corporation, R-1310-ARPA (in preparation).

Arthur, R. S., 1960, "A Review of the Calculation of Ocean Currents at the Equator," *Deep-Sea Res.*, 6, 287-297.

Bryan, Kirk, 1966, "A Scheme for Numerical Integration of the Equations of Motion on an Irregular Grid Free of Nonlinear Instability," *Mon. Weather Rev.*, 94, 39-40.

Bryan, Kirk, 1969a, "A Numerical Method for the Study of the Circulation of the World Ocean," *J. Comp. Phys.*, 4, 347-376.

Bryan, Kirk, 1969b, "Climate and the Ocean Circulation: III. The Ocean Model," *Mon. Weather Rev.*, 97, 806-827.

Bryan, Kirk, and M. D. Cox, 1967, "A Numerical Investigation of the Oceanic General Circulation," *Tellus*, 19, 54-80.

Bryan, Kirk, and M. D. Cox, 1968, "A Nonlinear Model of the Ocean Driven by Wind and Differential Heating," (Parts I and II), *J. Atmos. Sci.*, 945-978.

Bryan, Kirk, and M. D. Cox, 1972, "The Circulation of the World Ocean: A Numerical Study. Part I, A Homogeneous Model," *J. Phys. Oceanog.*, 2, 319-335.

Budyko, M. I., 1963, *Atlas of the Heat Balance of the Earth*, Gidrometeorizdat, Moscow, 69 pp.

Charney, J. G., 1955, "The Use of the Primitive Equations of Motion in Numerical Prediction," *Tellus*, 7, 22-26.

Charney, J. G., 1960, "Non-linear Theory of a Wind-driven Homogeneous Layer Near the Equator," *Deep-Sea Res.*, 6, 303-310.

Cox, M. D., 1970, "A Mathematical Model of the Indian Ocean," *Deep-Sea Res.*, 17, 47-75.

Crowley, W. P., 1968, "A Global Numerical Ocean Model: Part I," *J. Comp. Phys.*, 3, 111-147.

Eckart, Carl, 1958, "Properties of Water, Part II, The Equation of State of Water and Sea Water at Low Temperatures and Pressures," *Amer. J. Sci.*, 256, 225-240.

Gates, W. L., 1966, "On the Dynamical Formulation of the Large-Scale Momentum Exchange between Atmosphere and Ocean," *J. Marine Res.*, 24, 105-112.

Gates, W. L., 1968, "A Numerical Study of Transient Rossby Waves in a Wind-driven Homogeneous Ocean," *J. Atmos. Sci.*, 25, 3-22.

Gates, W. L., 1972a, "Numerical Studies of Transient Planetary Circulations in a Wind-driven Ocean," *Pure and Appl. Geoph.*, 99, 169-200.

Gates, W. L., 1972b, *The January Global Climate Simulated by the Two-Level Mintz-Arakawa Model: A Comparison with Observation*, The Rand Corporation, R-1005-ARPA, 107 pp.

Gates, W. L., E. S. Batten, A. B. Kahle, and A. B. Nelson, 1971, *A Documentation of the Mintz-Arakawa Two-Level Atmospheric General Circulation Model*, The Rand Corporation, R-877-ARPA, 408 pp.

Haney, R. L., 1971a, "A Numerical Study of the Large Scale Response of an Ocean Circulation to Surface Heat and Momentum Flux," Ph.D. Dissertation, Dept. of Meteorology, Univ. of Calif. at Los Angeles.

Haney, R. L., 1971b, "Surface Thermal Boundary Condition for Ocean Circulation Models," *J. Phys. Oceanog.*, 1, 241-248.

Hellerman, S., 1967, "An Updated Estimate of the Wind Stress on the World Ocean," *Mon. Weather Rev.*, 95, 607-626 (as corrected).

Houghton, David, and W. M. Washington, 1969, "On Global Initialization of the Primitive Equations: Part I," *J. Appl. Meteorol.*, 8, 726-737.

Kasahara, Akira, and W. M. Washington, 1971, "General Circulation Experiments with a Six-Layer NCAR Model," *J. Atmos. Sci.*, 28, 657-701.

Knauss, J. A., 1960, "Measurements of the Cromwell Current," *Deep-Sea Res.*, 6, 265-286.

Manabe, Syukuro, 1969, "Climate and the Ocean Circulation, II. The Atmospheric Circulation and the Effect of Heat Transfer by Ocean Currents," *Mon. Weather Rev.*, 97, 775-805.

Mintz, Yale, 1968, "Very Long-term Global Integration of the Primitive Equations of Atmospheric Motion: An Experiment in Climate Simulation," *Meteorological Monographs*, No. 30, 20-36.

Munk, W. H., 1950, "On the Wind-driven Ocean Circulation," *J. Meteorol.*, 7, 79-93.

Sarkisyan, A. S., and V. F. Ivanov, 1971, "Joint Effect of Baroclinicity and Bottom Relief as an Important Factor in the Dynamics of Sea Currents," *Bull. Acad. Sci. USSR, Atmos. and Ocean Phys.*, 7, 173-188.

Schutz, C., and W. L. Gates, 1971, *Global Climatic Data for Surface, 800 mb, 400 mb: January*, The Rand Corporation, R-915-ARPA, 173 pp.

Smagorinsky, J., S. Manabe, and J. L. Holloway, 1965, "Numerical Results from a Nine-Level General Circulation Model of the Atmosphere," *Mon. Weather Rev.*, 93, 727-768.

Smith, S. M., H. W. Menard, and George Sharman, 1966, *World-wide Ocean Depths and Continental Elevations*, Univ. of Calif., Scripps Institution of Oceanography, SIO Reference 65-8.

Sverdrup, H. U., M. W. Johnson, and R. H. Fleming, 1942, *The Oceans*, Prentice-Hall, Inc., New York, 1087 pp.

Warshaw, M., and R. R. Rapp, 1973, "An Experiment on the Sensitivity of a Global Circulation Model," *J. Appl. Meteorol.*, 12, 43-49.

Washington, W. M., and L. G. Thiel, 1970, *Digitized Global Monthly Mean Ocean Surface Temperatures*, National Center for Atmospheric Research, NCAR-TN-54, 30 pp.

Wyrtki, Klaus, 1964, *The Thermal Structure of the Eastern Pacific Ocean*, Deutsches Hydrographisches Institut, Hamburg, 84 pp.

Wyrtki, Klaus, and E. B. Bennett, 1963, "Vertical Eddy Viscosity in the Pacific Equatorial Undercurrent," *Deep-Sea Res.*, 10, 449-455.